Precambrian Research 305 (2018) 1–18

Contents lists available at ScienceDirect

Precambrian Research

journal homepage: www.elsevier.com/locate/precamres

Sveconorwegian vs. Caledonian orogenesis in the eastern Øygarden Complex, SW Norway – Geochronology, structural constraints and tectonic implications

Johannes D. Wiest[a,*], Joachim Jacobs[a,b], Anna K. Ksienzyk[a], Haakon Fossen[a,c]

[a] Department of Earth Science, University of Bergen, P.O. Box 7803, 5007 Bergen, Norway
[b] Norwegian Polar Institute, Fram Centre, P.O. Box 6606 Langnes, 9296 Tromsø, Norway
[c] Museum of Natural History, University of Bergen, P.O. Box 7803, 5007 Bergen, Norway

ARTICLE INFO

Keywords:
Baltica
Telemarkia
Sirdal Magmatic Belt
SIMS U–Pb zircon geochronology
Western Gneiss Region
Metamorphic core complex

ABSTRACT

The Øygarden Complex is the westernmost basement window in the Norwegian Caledonides, yet, the age and evolution of this part of the Baltic Shield is largely unknown. We examined the eastern part of the window by detailed field mapping and SIMS U–Pb zircon geochronology, to disentangle the record of Caledonian and Sveconorwegian orogenesis and to constrain the long-term crustal evolution. The eastern Øygarden Complex comprises mainly Sveconorwegian metaigneous rocks, which intrude Telemarkian granitic basement, dated at 1506 ± 5 Ma. Sveconorwegian magmatism occurred in two distinct phases: Contemporaneous hornblende biotite granite and gabbro intrusions revealed crystallization ages of 1042 ± 3 Ma and 1041 ± 3 Ma, respectively. We dated younger leucogranitic intrusions at 1027 ± 4 Ma, 1024 ± 6 Ma and ca. 1022 Ma. The new ages clearly identify the Øygarden Complex as a part of Telemarkia and correlate it with the Sirdal Magmatic Belt. Furthermore, they show that the Precambrian evolution of the Øygarden Complex is distinctly different from the Western Gneiss Region. Bimodal magmatism at 1041 Ma and the absence of Sveconorwegian high-grade metamorphism in the eastern Øygarden Complex support the idea of an accretionary Sveconorwegian orogen. Following long-term residence at low temperatures, a temperature increase caused resetting of high-U metamict zircons at ca. 482 Ma. This early Ordovician thermal event might reflect extension of the Baltican margin or early Caledonian convergence. Caledonian ductile reworking involved top-to-E shearing and recumbent lineation-parallel folding followed by the formation of ductile-to-brittle normal-sense shear zones. We discuss this structural evolution in the light of existing and new tectonic models, including early Devonian core-complex exhumation of the Øygarden Complex.

1. Introduction

Grenville-age orogens (1.3–1.0 Ga) are found on all continents and indicate a very important period of continental crust formation (Rino et al., 2008) that finally led to the formation of Rodinia (Li et al., 2008). Across the planet, the style of Grenville-age orogens ranges from large and hot continent-continent collision orogens to variably sized accretionary orogens (Cawood and Pisarevsky, 2017; Roberts et al., 2015). The Sveconorwegian orogen in southern Baltica is traditionally seen as a direct continuation of the Grenvillian continent-continent collision (e.g. Bingen et al., 2008b; Bingen et al., 2005; Möller et al., 2015). However, since the recent recognition of the late Mesoproterozoic (1050–1020 Ma) Sirdal Magmatic Belt in southern Norway (Coint et al., 2015; Slagstad et al., 2013a) the style of Sveconorwegian orogenesis has become a matter of controversy (Möller et al., 2013; Slagstad et al., 2013b). Previously, calc-alkaline 1040–1020 Ma granitoids in Telemarkia were interpreted as evidence of syn-collisional magmatism caused by crustal thickening (Bingen et al., 1993; Bingen and Van Breemen, 1998). Slagstad et al. (2013a,b), however, point out the subduction-related geochemical signatures of 1050–1020 Ma granitoids and the widespread absence of regional metamorphism and deformation after 1020 Ma in the Sirdal Magmatic Belt. Emplacement of the major granitic batholith was contemporary with mafic magmatism and voluminous mafic underplating (Bybee et al., 2014; Slagstad et al., 2017 and b). Based on these findings, Slagstad et al. (2013a) proposed a non-collisional and rather accretionary style of the Sveconorwegian orogen. Slagstad et al. (2017) argue that the Sveconorwegian province represents the lateral termination of the Grenvillian continent-continent

* Corresponding author.
E-mail address: johannes.wiest@uib.no (J.D. Wiest).

https://doi.org/10.1016/j.precamres.2017.11.020
Received 27 April 2017; Received in revised form 22 November 2017; Accepted 27 November 2017
Available online 27 November 2017
0301-9268/

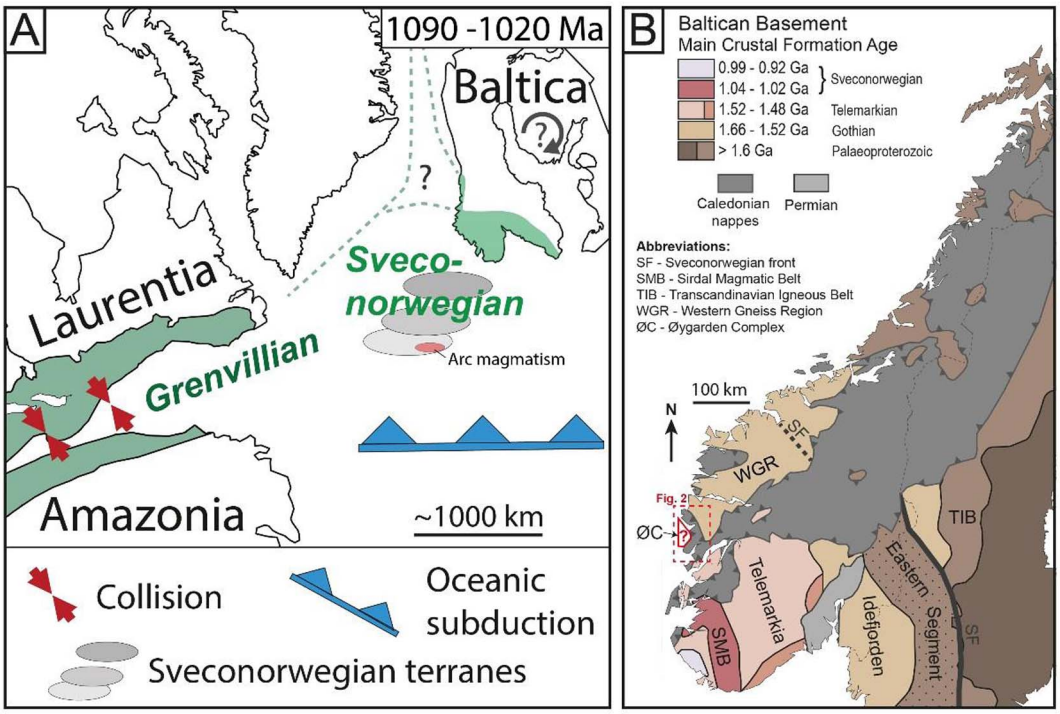

Fig. 1. A: Schematic paleogeography of Laurentia, Baltica and Amazonia for the period 1090–1020 Ma, showing the Sveconorwegian orogen as a lateral termination of the Grenville continent-continent collision modified from Slagstad et al. (2017). Possible clockwise rotation of Baltica (Cawood and Pisarevsky, 2017) is shown symbolically and a possible northward continuation of the Sveconorwegian belt (Gee et al., 2017) is indicated by green dashed lines. B: Simplified geologic map showing major tectonic units and crustal formation ages of the Baltic Shield. After Bingen and Solli (2009) and Slagstad et al. (2013a). Red rectangle marks extend of Fig. 2A. (For interpretation of the references to colour in this figure legend, the reader is referred to the web version of this article.)

collision, related to the spatially limited extent of the Amazonian continent (Fig. 1A). Cawood and Pisarevsky (2017) suggested a more dynamic model that is based on clockwise rotation of Baltica related to the opening of the Asgard Sea. In this alternative scenario, the southern margin of Baltica collided softly with Amazonia. However, the relationship between the Grenvillian and Sveconorwegian orogens is obscured by the loss or extensive tectonic reworking of vast parts of continental crust, which were originally linking the two orogenic belts (e.g. Gee et al., 2017). Large parts of the Sveconorwegian crust were strongly overprinted by the Caledonian orogeny (e.g. Gee et al., 2008). Therefore, tectonic models for the Sveconorwegian orogeny are based on a limited belt of preserved Precambrian crust as well as allochthonous fragments of Baltican crust (e.g. Roffeis et al., 2013). The Precambrian evolution of large parts of the 'caledonized' Baltican basement, on the other hand, remains poorly understood.

We address this problem by taking a closer look at the Øygarden Complex, the westernmost basement window in the Norwegian Caledonides (Fig. 2). The window exposes Precambrian rocks that experienced strong Caledonian reworking (Fossen and Rykkelid, 1992b; Sturt et al., 1975), but the precise age and origin of the pre-Caledonian protoliths are still unknown. The Øygarden Complex is located alongstrike of the Sirdal Magmatic Belt in the direction towards the Grenvillian orogen (Fig. 1), making it a key area for our understanding of Sveconorwegian orogenesis. In this study, we test a possible Grenville-age affinity of the Øygarden Complex after carefully disentangling its strong Caledonian overprint. Thereby, we try to clarify the relationship between the Øygarden Complex and adjacent basement provinces as well as the Sirdal Magmatic Belt. Detailed field mapping in the eastern Øygarden Complex constrained igneous and metamorphic as well as structural relationships, and formed the basis for Secondary Ion Mass Spectrometry (SIMS) U-Pb zircon geochronology. This paper presents a detailed geologic description of the eastern Øygarden Complex and the first high-resolution U–Pb zircon geochronological data from the entire Øygarden Complex.

2. Geologic setting

2.1. Precambrian evolution of SW Norway

Most of the Baltican continental crust formed in the Proterozoic at the long-lived (1.9–0.9 Ga) accretionary margin of Fennoscandia (Bingen and Solli, 2009; Roberts and Slagstad, 2015; Torsvik and Cocks, 2005). This evolution is reflected in the distribution of main crustal formation ages in Scandinavia, getting generally younger from E towards W (Fig. 1B). In SW Norway, the basement can be principally subdivided into a Gothian (1.66–1.52 Ga) and a Telemarkian (1.52–1.48 Ga) domain (Bingen et al., 2005). The Gothian-Telemarkian orogenic episode marks a distinct period of spatially and temporally variable arc magmatism, sedimentation and accretion in a subduction-zone environment at the long-lived accretionary margin of Fennoscandia (Roberts and Slagstad, 2015). Gothian crust constitutes the Western Gneiss Region (WGR) and the Idefjorden Terrane (e.g. Rohr et al., 2013; Skår, 2000; Skår et al., 1994; Skår and Pedersen, 2003). In contrast, 1.52–1.48 Ga crust and a significant volume of Sveconorwegian intrusives (1.15–0.9 Ga) define Telemarkia and the Bamble-Kongsberg terrane (e.g. Bingen et al., 2008a,b; Bingen and Solli, 2009; Coint et al., 2015; Slagstad et al., 2013a). The Sveconorwegian orogeny marks the final episode of the long-lived accretionary history at the active SW margin of Fennoscandia (Roberts and Slagstad, 2015). Sveconorwegian tectonics juxtaposed different crustal blocks and largely formed the internal structure of the Baltican basement (Bingen et al., 2005), yet, the style of the Sveconorwegian orogeny remains controversial (e.g. Bingen et al., 2008b; Möller et al., 2013; Slagstad et al., 2017; Slagstad et al., 2013a,b). Rodinia's break up around 800 Ma was followed by the opening of the Iapetus Ocean from around 550 Ma, with Baltica emerging as an independent continent (Cocks and Torsvik, 2005; Li et al., 2008; Pease et al., 2008; Torsvik and Cocks, 2005). Multiple phases of extension apparently led to the formation of a hyperextended margin of Baltica (Abdelmalak et al., 2015; Andersen

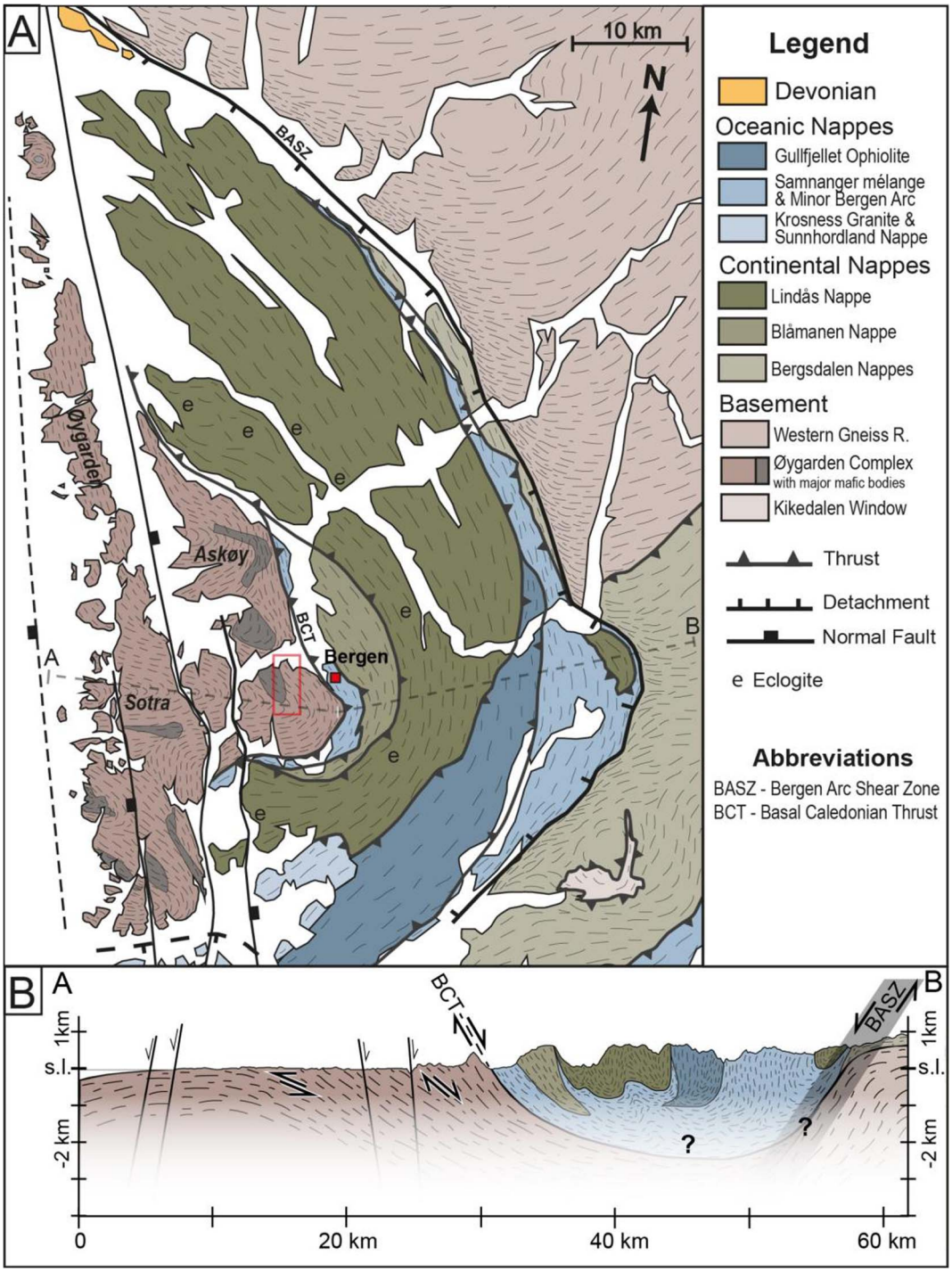

Fig. 2. A: Simplified geologic map of the Bergen Arc System based on Ragnhildstveit and Helliksen (1997). Dashes indicate the trace of foliation and the red rectangle marks the study area around Mt. Lyderhorn. B: Schematic E-W cross section through the Bergen Arc System based on Ragnhildstveit and Helliksen (1997) and Fossen (1998). The present geometry of the Basal Caledonian Thrust (BCT), which separates the Øygarden Complex from the overlaying nappes, could be explained either by passive rotation or by reactivation as a detachment. (For interpretation of the references to colour in this figure legend, the reader is referred to the web version of this article.)

et al., 2012; Jakob et al., 2017).

2.2. Paleozoic evolution of the Baltoscandian margin

From around 480 Ma, the Caledonian orogeny evolved around the closure of the Iapetus Ocean and resulted in Scandian (Silurian) oblique continent-continent collision between Laurentia and Baltica (Gee, 1975; Gee et al., 2008; Roberts, 2003; Torsvik and Cocks, 2005). Various early Caledonian events are recorded in different allochthonous units, but their allocation to either the Baltican or the Laurentian margin is in many cases controversial (e.g. Corfu et al., 2014; Faerseth et al., 2011; Roberts, 2003; Sturt et al., 1978). At the Laurentian margin, several Ordovician ophiolite complexes were emplaced in a suprasubduction setting, accompanied by arc magmatism, accretion and subduction of transitional Laurentian crust (Taconic orogeny; e.g. Andresen and Steltenpohl, 1994; Augland et al., 2014; Dunning and Pedersen, 1988; Furnes et al., 2012; Pedersen and Dunning, 1997; Slagstad et al., 2014; Steltenpohl et al., 2003). Early subduction of previously rifted parts of

the Baltoscandian margin is recorded in Ordovician ultra-high pressure rocks in some Caledonian thrust nappes (e.g. Brueckner et al., 2004; Essex et al., 1997; Gee et al., 2013; Hacker and Gans, 2005; Klonowska et al., 2014; Root and Corfu, 2012).

During the Scandian phase, the Baltican margin was deeply subducted below Laurentia, reaching ultra-high pressure conditions in parts of the WGR (Hacker et al., 2010; Root et al., 2004). The metasedimentary basement cover acted as the basal décollement for a wedge-shaped pile of nappes that was thrust onto the Baltoscandian margin to the SE (Gee, 1975; Gee et al., 2008). Post-orogenic extensional deformation strongly affected the Scandinavian Caledonides (Fossen, 2010). During Mode I extension, the basal décollement zone was reactivated with top-to-the-hinterland (NW) transport (Fossen, 1992, 2000; Fossen and Dunlap, 1998), corresponding to eduction of the Baltican slab (Andersen et al., 1991). Subsequent Mode II extension formed steeper hinterland-dipping extensional shear zones that cut through the orogenic wedge and the inactivated décollement zone and rapidly exhumed the basement to shallow crustal depths (e.g. Andersen and Jamtveit, 1990; Fossen, 1992; Fossen and Hurich, 2005; Milnes et al., 1997; Norton, 1987) . Intermontane basins filled with Middle Devonian conglomerates and sandstones formed in the hanging wall of the Nordfjord-Sogn Detachment Zone (Johnston et al., 2007; Seranne and Seguret, 1987; Steel et al., 1985; Vetti and Fossen, 2012) and the Bergen Arc Shear Zone (Wennberg et al., 1998). The detachments, high-grade footwall gneisses as well as the supra-detachment basins were folded into E-W-trending upright folds in a transtensional regime (Chauvet and Seranne, 1994; Fossen et al., 2016; Fossen et al., 2013; Krabbendam and Dewey, 1998; Osmundsen and Andersen, 2001). The onset of brittle extensional deformation (Mode III) has been dated in the Bergen area to 396 Ma (Larsen et al., 2003). At the same time, partial melting continued in the WGR (Gordon et al., 2013). Brittle conditions were reached in parts of the WGR as late as the Permian, according to Eide et al. (1997).

2.3. The Øygarden Complex

The Øygarden Complex forms a tectonic window occupying the core and the western part of the Bergen Arc System (Fig. 2; Johns, 1981; Kolderup and Kolderup, 1940). The Bergen Arcs consist of a series of Caledonian nappes with different origins and tectonic histories, which are synclinally folded and refolded into a large-scale arc structure (Fossen, 1989; Kvale, 1960; Sturt and Thon, 1978). The allochthons occupy a major depression in the basement (Fig. 2B; Fossen and Dunlap, 2006) which is related to the Bergen Arc Shear Zone (BASZ), a Devonian extensional shear zone (Fossen and Rykkelid, 1992a; Wennberg and Milnes, 1994; Wennberg et al., 1998). Basement rocks in the footwall of the concave-shaped BASZ are considered part of the southern WGR. The Øygarden Complex comprises (par)autochthonous basement in the hanging wall of the shear zone (Kvale, 1960; Ragnhildstveit and Helliksen, 1997; Sturt et al., 1975). However, due to strong penetrative deformation of the Øygarden Complex, an allochthonous state has also been suggested (Bering, 1985).

The rocks in the Øygarden Complex are mainly granitic, granodioritic and tonalitic gneisses as well as several bodies of gabbroic rocks, which are mostly transformed into amphibolites (Johns, 1981). The only published geochronological ages, so far, are Rb/Sr whole rock ages that show a large scatter ranging from 1750 to 473 Ma (Sturt et al., 1975). SIMS U–Pb analysis of three single zircon grains revealed a poorly constrained upper intercept age of 1620 ± 120 Ma (Knudsen and Fossen, 2001). Johns (1981) suggested that most gneisses and amphibolites in the Øygarden Complex are Pre-Svecofennian (> 1800 Ma) and represent a meta-volcanic-sedimentary succession. Gabbroic and granitic rocks in the Haganes gneissose granite suite on Sotra (Fig. 2A) partially preserve intrusive relationships and revealed Sveconorwegian Rb–Sr ages (Johns, 1981; Sturt et al., 1975). These rocks have been correlated with a large gabbroic pluton on Askøy (Askvik, 1971) and the arc-shaped belt of augen gneisses that forms the eastern limit of the Øygarden Complex (Weiss, 1977). In some of the granitic rocks within the latter group, exceptionally high radiogenic heat production values have been recently discovered (Pascal and Rudlang, 2016; Schulze, 2014).

Thermochronological studies in the western part of the Øygarden Complex showed that Scandian peak metamorphism reached upper amphibolite facies conditions with temperatures in excess of 650 °C at 7–8 kbar (Boundy et al., 1996). They were followed by rapid exhumation in the early Devonian through lower amphibolite facies at 408–404 Ma and greenschist facies at 401 Ma to the brittle-plastic transition at 396 Ma (Boundy et al., 1996; Fossen and Dunlap, 1998; Larsen et al., 2003). Besides basic field studies conducted by Askvik (1971) and Weiss (1977), neither detailed structural nor thermochronological constraints are available from the eastern Øygarden Complex so far. Generally, the mylonitic contact between the Øygarden Complex and the Paleozoic rocks of the Minor Bergen Arc is considered as the basal Caledonian thrust (Fossen, 1989; Kvale, 1960) and top-to-E fabrics in the eastern Øygarden Complex are accordingly interpreted to reflect Scandian southeastward thrusting (Fossen and Dunlap, 1998; Larsen et al., 2003; Wennberg, 1996). In contrast to the basal décollement of the SW Norwegian Caledonides farther east, this segment of the basal thrust was not reactivated with top-to-NW deformation corresponding to Mode I extension (Fossen, 1993; Fossen and Dunlap, 1998). Structurally lower levels in the western part of the Øygarden Complex, on the other hand, record strong ductile top-to-W shearing related to early Devonian crustal extension (Fossen and Rykkelid, 1992a; Rykkelid and Fossen, 1992). The main composite gneissic fabric in the Øygarden Complex is folded into a series of upright E-plunging syn- and antiforms (Fig. 2A), including top-to-W fabrics (Fossen and Rykkelid, 1990). The general eastward dip of the gneissic fabrics becomes progressively shallower towards the west and rotates into shallow westward dip at the westernmost shoreline, reflecting a large N–S-trending anticline (Fig. 2C; Fossen, 1998; Larsen, 1996; Larsen et al., 2003). Steep brittle faulting and the intrusion of N–S-trending basaltic dykes are related to various phases of Mesozoic rifting (e.g. Fossen, 1998; Fossen et al., 2016; Ksienzyk et al., 2014; Ksienzyk et al., 2016; Larsen et al., 2003).

3. High-resolution field mapping of the eastern Øygarden Complex

Directly west of the city of Bergen, the mountains Lyderhorn, Damsgårdsfjellet and Løvstakken form a horseshoe-shaped belt, mostly consisting of granitic rocks (sometimes referred to as the “Løvstakken granite”) that follows the contact between Øygarden Complex and Minor Bergen Arc (Weiss, 1977). The 400 m-high mountain Lyderhorn (Figs. 2 and 3) forms an N–S-elongated ridge with steep eastern and western flanks, which offer excellent and easily accessible exposures. Based on lithological differences, five metaigneous lithological units have been identified (Table 1) and are shown on the newly compiled detailed geologic map (Fig. 3).

3.1. Lithological field relationships

The northern ridge of the mountain consists of a layered sequence of granitic, granodioritic and tonaltitic gneisses that are variably deformed, ranging from coarse-grained granites to mylonites. Local amphibolite dykes are concordant to the foliation without clear cross-cutting relationships. A major body of gabbroic rocks that has been mostly metamorphosed and transformed into metagabbros and amphibolites occupies the central part of the study area. Minor lenses that escaped deformation show an original noritic composition, indicating that the basic body can be correlated with the nearby norite pluton on Askøy (Fig. 2A; Askvik, 1971). Different types of granites intrude the gabbroic rocks. Hornblende biotite granite gneiss forms two confined

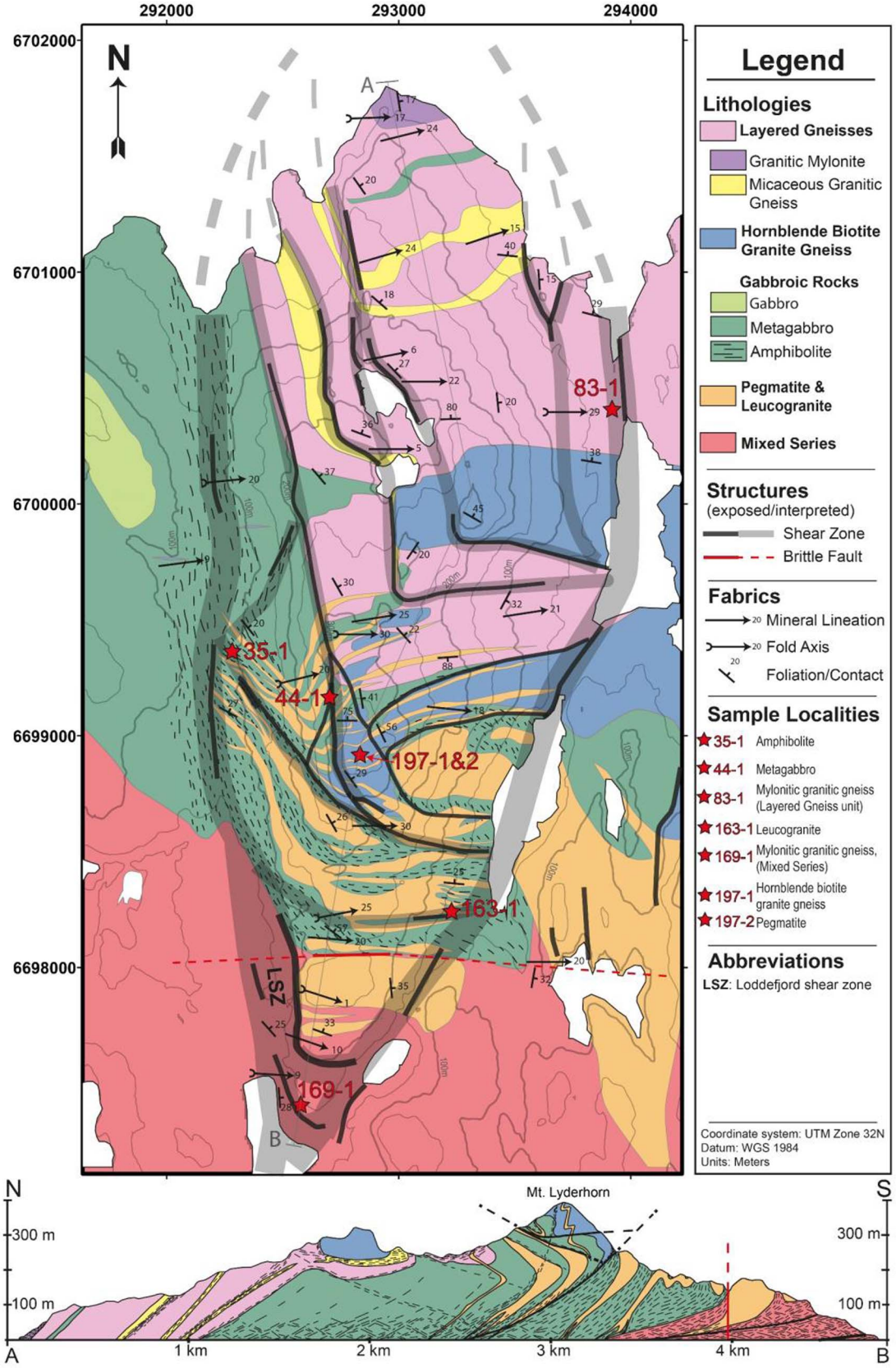

Fig. 3. Newly compiled geologic map and N–S cross section of the Lyderhorn area in the eastern Øygarden Complex showing sample localities for U–Pb zircon geochronology. Note that the shear zone pattern reflects the topography of the mountain, which relates to shallowly E-dipping shear zones and steep N–S- and E–W-trending brittle faults.

Table 1
Lithological units and SIMS U–Pb zircon geochronology samples.

Unit	Lithologies	Sample	Igneous Age	GPS Position
Layered gneisses	**Mylonitic granitic gneiss** Granitic augen gneiss Micaceous granit. gneiss Tonalitic gneiss	LYD-83-1	1506 ± 5 Ma	5°15′35,7″E, 60°23′14,5″N
Gabbroic rocks	Gabbro **Metagabbro** **Amphibolite**	 LYD-44-1 LYD-35-1	 1041 ± 3 Ma 1040 ± 11 Ma	 5°14′20,9″E, 60°22′31,9″N 5°13′53,6″E, 60°22′37,7″N
Hornblende biotite granite gneiss	**Hornblende biotite granite gneiss**	LYD-197-1	1041 ± 3 Ma	5°14′30,7″E, 60°22′24,9″N
Pegmatite and leucogranite	**Leucogranitic pegmatite** **Gneissic leucogranite**	LYD-197-2 LYD-163-1	1022 ± 11 Ma 1022 ± 11 Ma	5°14′30,7″E, 60°22′24,9″N 5°14′58,5″E, 60°22′4,5″N
Mixed Series	Leucogranitic pegmatite **Mylonitic granitic gneiss** Amphibolite Hornblende biotite granite gneiss	 LYD-169-1	 1027 ± 4 Ma	 5°14′18,8″E, 60°21′37,5″N

bodies and show a gradual transition towards tonalite at the margins of the intrusions. Locally, hornblende biotite granite clearly intrudes gabbroic rocks (Fig. 4A), but more commonly the contacts are interlayered zones with ambiguous relationships, which imply that the granite intruded the gabbro before the latter was entirely crystallized. Leucogranites and pegmatites intrude all the previously described units and form E-W striking dykes that get increasingly more voluminous towards the south. Compositions range from alkali feldspar granite to monzogranite, and textures vary gradually from pegmatitic to medium-grained granitic gneiss. The mapped occurrence of the leucogranites and pegmatites coincides precisely with high concentrations of radioactive elements, found through gamma-spectrometry measurements carried out by Schulze (2014). In the southernmost part of the study area, the previously described lithologies alternate on a meter-scale with the dominant leucogranitic gneisses. Lenses of amphibolite and metagabbro are contained within layers of hornblende biotite granite gneiss and banded mylonitic granitic gneisses. Abundant K-feldspar-rich leucogranitic pegmatites show clear intrusive relationships with the other lithologies. The unit is here termed Mixed Series, following Weiss (1977) who mapped the unit as 'layered series'. The strong mixing of lithologies appears to be related to intrusive relationships in combination with strong tectonic transposition.

3.2. Metamorphic fabrics and mineralogy

To various degrees, all the magmatic lithologies were affected by metamorphic recrystallization and transformed into L, L > S or L = S tectonites. Metamorphosed and deformed gabbroic rocks clearly show that peak metamorphism reached amphibolite facies conditions. Metagabbros consist mostly of plagioclase and green hornblende overgrowing relict orthopyroxene, with minor amounts of biotite, titanite-rutile aggregates and epidote. In areas of higher strain, metagabbros grade into amphibolites, which are mineralogically similar but characterized by finer grain size, the absence of pyroxenes and the local occurrence of garnet. Recrystallized plagioclase and aligned growth of hornblende form a pronounced E-plunging mineral lineation in mylonitic amphibolites (Fig. 4B).

Metagranitic rocks range from protomylonites to ultramylonites and show heterogeneous, but generally, strong dynamic recrystallization of quartz and feldspar. Elongated rods of recrystallized quartz and feldspar form a well-defined shallowly E-plunging linear fabric in most granitic rocks while the development of a mylonitic foliation is more heterogeneous (Fig. 4C): Foliations are well developed within anastomosing shear zones and in mica-rich lithologies, however, augen gneisses with a dominant L fabric are abundant. Microfabrics in metagranitic rocks show mostly deformation at greenschist facies conditions, but amphibolite facies fabrics occur in banded gneisses. Metamorphic index minerals that could constrain peak metamorphic conditions more precisely are absent. Leucogranites and pegmatites are commonly rich in K-feldspar and exhibit heterogeneous mineral-dependent deformation at greenschist facies conditions (Fig. 4D), i.e. quartz domains show strong dynamic recrystallization, while K-feldspar crystals are only marginally recrystallized and deform mainly by brittle fracturing. In places, feldspathic pegmatites appear to have escaped ductile deformation probably due to strain partitioning into more quartz- or mica-rich lithologies.

A characteristic feature of the area is the intensity of low-grade deformation and alteration. Cataclastic fabrics are abundant in shallowly E-dipping high-strain zones, which exhibit a strong brittle overprint on previously ductile fabrics (see section 3.4). Within this ductile-to-brittle shear zones retrograde hydration mineral reactions indicate the presence of fluids during deformation at greenschist facies and even lower metamorphic grades (Wintsch et al., 1995). Chlorite phyllonites formed from mafic rocks, where biotite replaced amphibole and was itself altered into chlorite (Fig. 4E). In felsic phyllonites that formed from granitic rocks, K-feldspar was largely replaced by muscovite and quartz (Fig. 4G–H). The strain weakening that is associated with these retrograde mineral reactions (Bos and Spiers, 2002) enhanced the localization of low-grade deformation in discrete shear zones. Further evidence for hydrothermal activity at greenschist facies conditions in high-strain zones can be found at several locations. In a mylonitic to cataclastic granitic fault rock, garnet porphyroblasts overgrow muscovite and quartz, which themselves replace K-feldspar (Fig. 4F). Radial aggregates of actinolite have been found overgrowing granitic fragments in a chlorite breccia and in most thin section samples abundant saussuritization of plagioclase and kaolinitization of K-feldspar can be observed.

3.3. Fabric orientation, kinematic indicators and fold geometries

Shallow eastward dipping planar fabrics and ENE-plunging linear fabrics characterize the structural geometry of the study area with a distinct appearance of E–W and N–S outcrop faces (Fig. 5A). In sections parallel to the E-plunging mineral stretching lineations, fabrics appear with mostly subhorizontal preferred orientations and are rotated into parallelism. On the other hand, sections perpendicular to the lineation exhibit contrasting domains with predominant linear or planar fabrics, respectively. L > S domains are characterized by prolate feldspar augen as well as ribbons of recrystallized quartz and feldspar that could indicate constriction. The preservation of primary intrusive

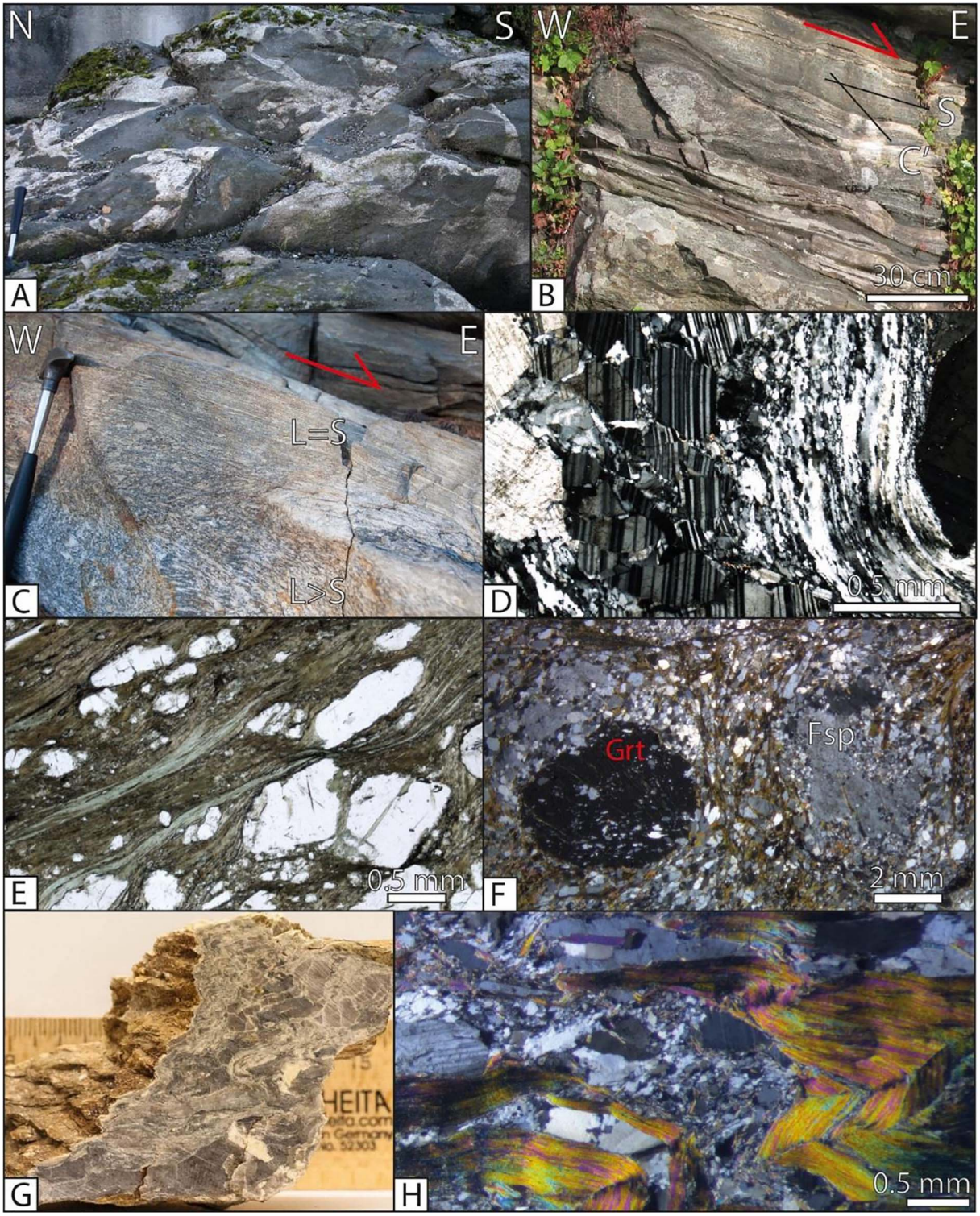

Fig. 4. Photographs of field relationships and metamorphic fabrics. A: Bright hornblende biotite granite veins intruding amphibolite (60°22′55.58″N; 5°13′56.30″E) seen in section perpendicular to mineral lineation. B: Mylonitic amphibolite in section parallel to the mineral lineation (60°21′34.07″N; 5°14′27.75″E). C′-shear bands deflect the mylonitic foliation (S) and indicate top-to-E sense of shear. C: Mesoscale shear zone in mylonitic granitic gneiss (60°23′18.11″N; 5°14′24.57″E). A mylonitic foliation is well developed within the shear zone (L = S), while the gneiss in the footwall has a dominant L fabric. Deflection of the foliation and asymmetrically sheared feldspar clasts indicate top-to-E sense of shear. D: Photomicrograph (crossed polarized light) of granite pegmatite showing strong dynamic recrystallization of quartz and brittle fracturing of plagioclase. E: Photomicrograph (plain polarized light) of chlorite phyllonite (same as Fig. 6E). F: Photomicrograph (crossed polarized light) of granitic fault rock (60°23′6.92″N; 5°14′56.96″E) showing unstable K-feldspar being replaced by quartz and muscovite close to a large garnet porphyroblast. G: Cut hand specimen of felsic phyllonite (60°22′17.74″N; 5°14′34.86″E), showing almost complete replacement of K-feldspar (yellowish-white) by muscovite and quartz. H: Photomicrograph (crossed polarized light) of the same fault rock. (For interpretation of the references to colour in this figure legend, the reader is referred to the web version of this article.)

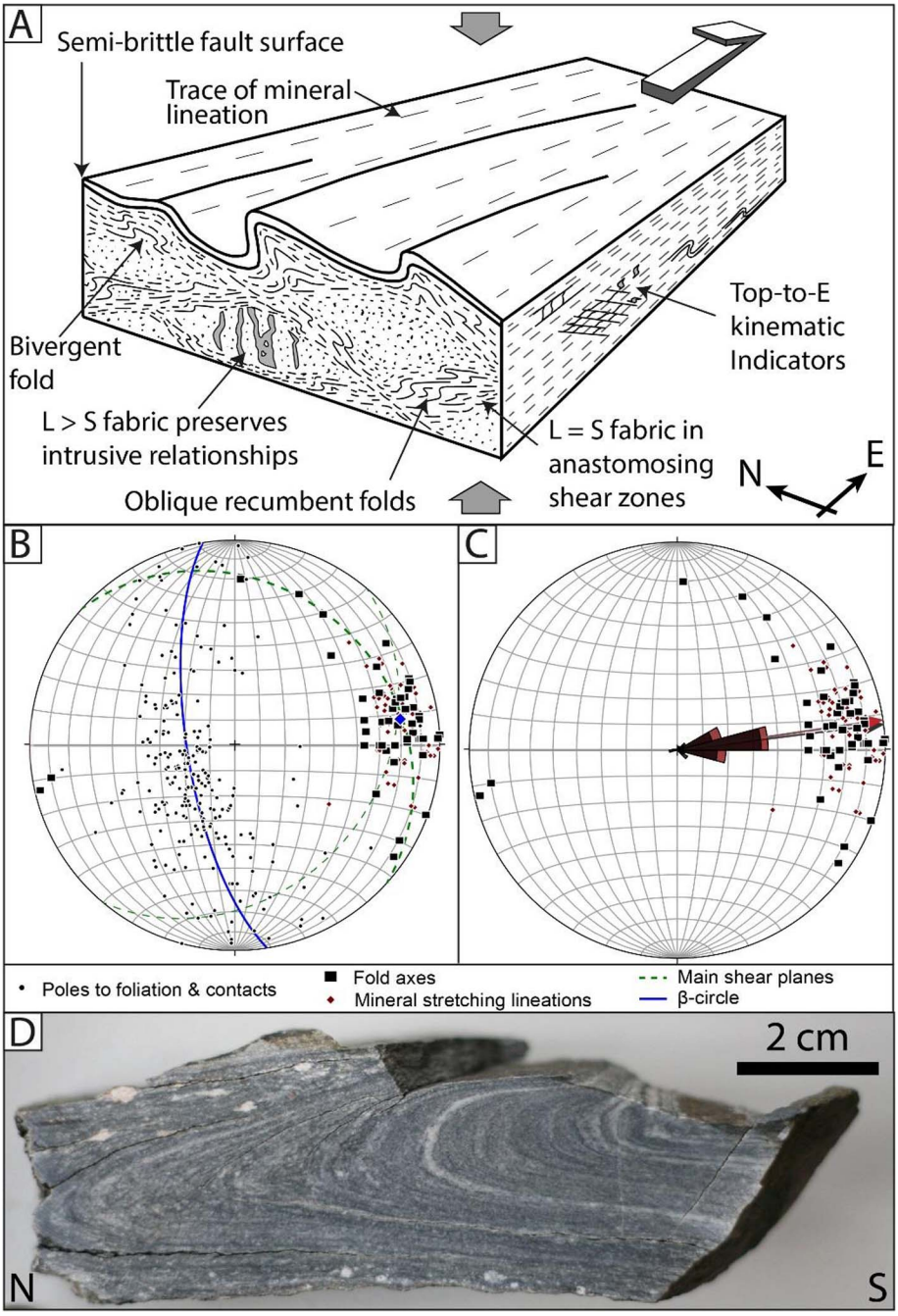

Fig. 5. A: Schematic drawing illustrating the style of ductile deformation. See text for discussion B: Lower hemisphere equal-area plot of measured linear and planar fabrics. The plot was created with Stereoplot (Allmendinger et al., 2011). C: Lower hemisphere equal-area plot of mineral lineations (red, n = 64) and fold axes (black, n = 52) showing rose diagrams and calculated mean trends (arrows). Both populations have an identical mean trend of 82°. D: Cut hand specimen of a cylindrical isoclinal recumbent fold in mylonitic granitic gneiss. The orientation of the fold axis (15 → 074) is parallel to the mineral lineation defined by elongated rods of recrystallized quartz and feldspar. (For interpretation of the references to colour in this figure legend, the reader is referred to the web version of this article.)

relationships in the L > S domains and the geometric relationship between all measured fabric elements with consistent orientations indifferent of metamorphic grade (Fig. 5B) indicate that all of the fabrics seem to be related to one main deformation event. In outcrop sections parallel to the mineral lineation, abundant kinematic indicators are well developed. S-C′ type structures (Figs. 4B and 6D), deflected mylonitic foliations (Fig. 4C), asymmetrically sheared clasts (Fig. 6C) as well as E-vergent isoclinal folds show without exception non-coaxial strain with top-to-E(NE) sense of shear from amphibolite facies to lowest greenschist facies conditions.

The mylonitic foliation and contacts between all the different lithologies exhibit strong folding on various scales. Planar fabrics exhibit folding around an ENE-plunging fold axis (Fig. 5B), and the general NE-dip reflects the position of the study area on the northern limb of an upright, E-plunging megafold (Weiss, 1977). Observable meso- and macrofolds can be grouped into two sets based on different geometries and orientations. A minor set of N–S-trending, E-vergent, isoclinal recumbent folds are commonly non-cylindrical with strongly curved hinge lines and non-planar axial surfaces. Far more abundant are ENE-plunging tight to isoclinal recumbent folds that are mostly cylindrical on the outcrop scale and classify as parallel folds with attenuated limbs and thickened hinge areas (Fig. 5D). This set of folds has subhorizontal axial surfaces that dip to the North, as well as the South, creating in places bivergent fold patterns in single layers (Fig. 5A). Statistically, the orientation of the acquired fold axes and mineral stretching lineations is identical; both have a mean trend of 82° (Fig. 5C). Folded mylonitic foliations, which are cut by discrete top-to-E shear zones with lower greenschist facies fabrics (see below), indicate that the recumbent lineation-parallel folds formed most likely simultaneously with amphibolite to upper-greenschist facies top-to-E shearing. Assuming that the recumbent mesofolds and the upright megafold (Weiss, 1977) formed at the same time, their relationship

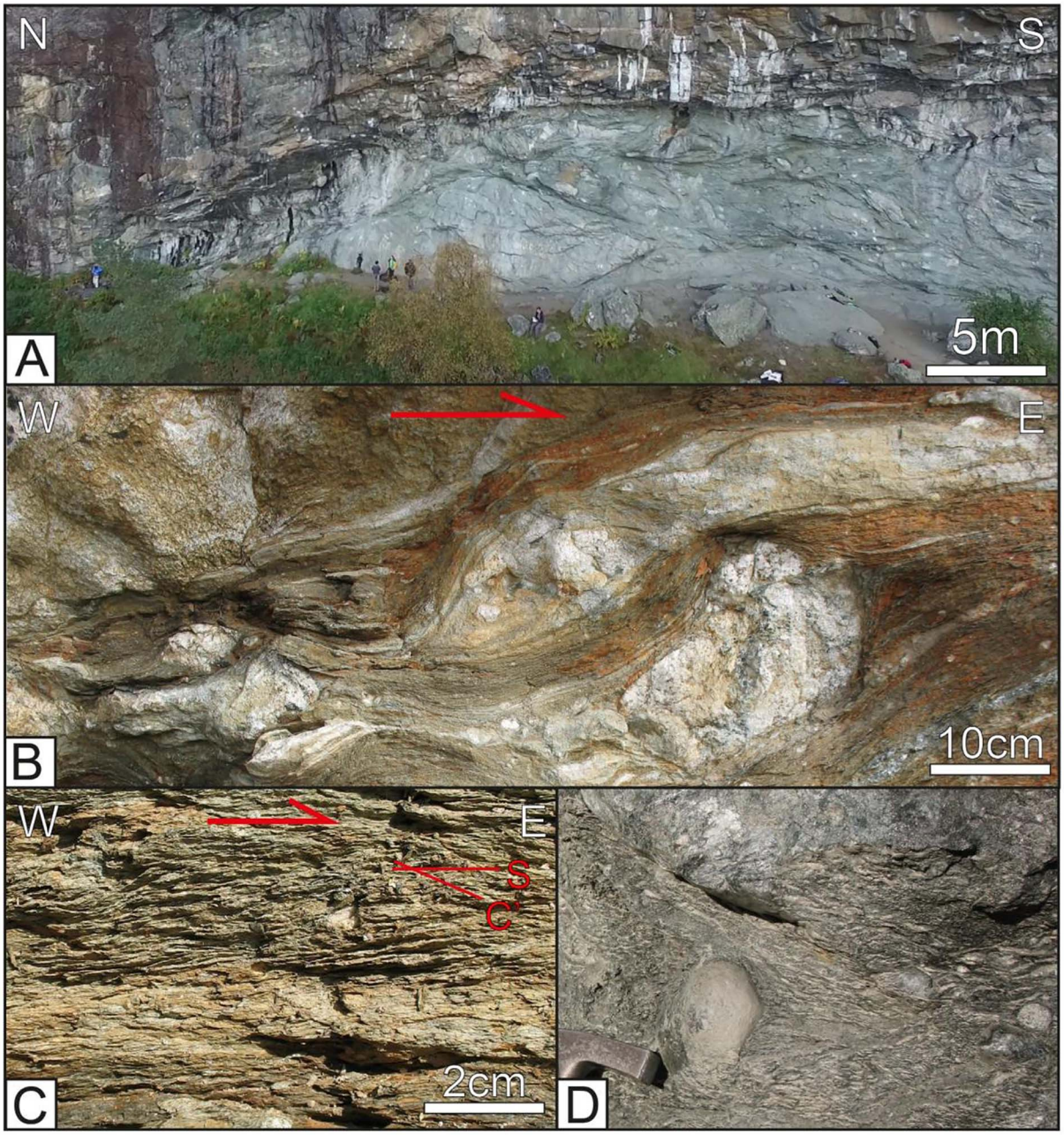

Fig. 6. Loddefjord shear zone: A: View of the main deformation zone in section perpendicular to the mineral lineation (60°21′46.50″N; 5°14′17.10″E). Within the deformation zone, granitic fragments float in a matrix of chlorite phyllonite. Drone image from Robert Sasak. B and C: Field photographs of shallowly E-dipping fabrics in section parallel to the mineral lineation (60°21′42.69″N; 5°14′19.39″E). Asymmetrically sheared granitic clasts and C′-S structures within the phyllonitic matrix indicate top-to-E sense of shear. D: Strongly rounded granitic clasts in the "tectonic conglomerate".

corresponds to the geometry of cascading folds (Whitney et al., 2004) and indicates that the area was affected by vertical shortening on a regional scale.

3.4. Ductile-to-brittle low-angle shear zones

Numerous shallowly NE- and SE-dipping shear zones with top-to-E displacement dissect the entire study area and cut earlier formed fold structures (Fig. 3). The pattern of shear zones on the geologic map is caused by the intersection of E-dipping shear zones with subvertical N–S- and E–W-striking brittle faults. High-strain zones exhibit relict amphibolite facies fabrics, but most deformation occurred at greenschist facies conditions and continued, enhanced by retrograde strain-weakening hydration reactions (section 3.2), to semi-brittle conditions.

The Loddefjord Shear Zone, which consists of several anastomosing branches at the western base of the mountain Lyderhorn (Fig. 3), provides excellent exposures to study shear zone evolution (Fig. 6). Strain localization at amphibolite and upper greenschist facies deformation was facilitated by abundant intrusive contacts in the Mixed Series, which are associated with strong rheological contrasts. The alteration of amphibolites into chlorite phyllonites allowed strain localization into mafic layers at lower metamorphic grades. The deformation zone of the Loddefjord Shear Zone is of variable thickness, reaching up to 10 m, and contains fragments of granitic and tonalitic gneiss floating in a matrix of greenish-grey chlorite phyllonite (Fig. 6A). Linear fabrics are defined by the preferred orientation of amphiboles in mylonitic amphibolite, quartz-feldspar rods in granitic gneiss as well as biotite and chlorite in the phyllonitic matrix and plunge consistently shallowly to the East. In

Fig. 7. Geochronology sample lithologies and representative CL images of analyzed zircon grains. Note the distinct textures of zircons from granitic (A, D, E), gabbroic (B, C) as well as highly radioactive leucogranitic samples (A, F), respectively. Analyzed spots (15 µm diameter) are shown by red circles together with resulting single grain Concordia ages. Note that discordant ages (grey) are not geologically significant. (For interpretation of the references to colour in this figure legend, the reader is referred to the web version of this article.)

addition, quartz-striations on corrugated shallowly E-dipping brittle fault surfaces show an identical orientation. In sections parallel to the lineation, asymmetrically sheared granitic clasts, E-vergent folding of the mylonitic foliation, as well as S-C structures in the phyllonitic matrix indicate uniformly top-to-E sense of shear (Fig. 6B and C). In other exposures, ductile flow of the phyllonitic matrix caused brecciation of granitic fragments and created a peculiar-looking fault rock with strongly rounded clasts, which consist of isolated fold hinges (Fig. 6D). Kolderup and Kolderup (1940) coined the term 'tectonic conglomerate' that has been used to describe similar fault rocks from various parts of the Øygarden Complex (Johns, 1981; Weiss, 1977).

4. SIMS U–Pb zircon geochronology

4.1. Samples and methods

Seven metaigneous samples were collected from key localities to represent the previously identified lithological units, as well as different states of deformation, comprising orthogneisses, gneissic leucogranite, pegmatite, metagabbro and amphibolite (Table 1; Figs. 3 and 7). Mineral separation at the University of Bergen followed standard procedures. Separated zircon grains were handpicked, mounted in epoxy and polished prior to cathodoluminescence (CL) imaging using a ZEISS SUPRA 55VP SEM (scanning electron microscope) at the University of Bergen. U–Pb geochronology was performed using a CAMECA IMS1280 large-geometry ion microprobe at the NordSIMS facility, Stockholm, following routine procedures outlined by Whitehouse et al. (1999) and Whitehouse and Kamber (2005): A ca. 6 nA, −13 kV O_2^- primary beam (imaged aperture of 150 µm corresponding to a spot diameter on the sample of ca. 15 µm) was used to sputter +10 kV secondary ions, which were admitted to the mass spectrometer and detected in a peak-hopping sequence using a single ion-counting electron multiplier (EM). The mass spectrometer was operated at a mass resolution (M/ΔM) of 5400, sufficient to separate all species of interest from molecular interferences. Each analysis comprised a 70 s pre-sputter to remove the Au coating and allow the secondary beam to stabilize, centering of the secondary beam in the field aperture, energy optimization in the 45 eV energy window, mass calibration adjustment using the $^{90}Zr_2{}^{16}O$ peak, and 12 cycles through the species of interest. Groups of analyses were performed in fully automated sequences, regularly interspersing reference

material analyses with those of the sample zircon grains. Data reduction utilized an in-house developed suite of software. Pb-isotope ratios were corrected for common Pb estimated from measured ^{204}Pb assuming the present-day terrestrial Pb isotope composition calculated with the model of Stacey and Kramers (1975), except where the ^{204}Pb count was statistically insignificant relative to the long-term background on the EM, in which case no correction was applied. U/Pb ratios were calibrated using a Pb/UO–UO_2/UO calibration (Jeon and Whitehouse, 2015) from regular measurements of the 1065 Ma 91500 zircon (Wiedenbeck et al., 1995). Age calculations assume the decay constant recommendations of Steiger and Jäger (1977) and utilize the routines of Isoplot-Ex (Ludwig, 2003). All age uncertainties include uncertainties on the decay constants as well as propagation of the error on the Pb/UO–UO_2/UO calibration (Jeon and Whitehouse, 2015; Whitehouse et al., 1997), and are reported at 2σ if not further specified. For Concordia ages, the mean square of weighted deviates (MSWD) on combined equivalence and concordance is reported following the recommendation of Ludwig (1998). Zircon U–Pb data are presented in Appendix A: Table S1.

4.2. U–Pb geochronology results

4.2.1. Hornblende biotite granite gneiss (LYD-197-1)

Weakly foliated hornblende biotite granite gneiss was sampled at the peak of Lyderhorn (Fig. 3) where it is intruded by a subvertical pinkish pegmatite dike that constitutes sample LYD-197-2 (Fig. 7A). The rock consists mostly of coarse grained K-feldspar augen surrounded by a matrix of fine grained, dynamically recrystallized quartz, plagioclase and biotite. Large blueish-green hornblende phenocrysts form mafic clusters together with biotite and rutile. The analyzed zircon crystals are large (100–300 µm), idiomorphic (aspect ratio 3–4), transparent and show oscillatory zoning in CL images, as is typical for zircon crystallized from granitic melts (Corfu et al., 2003). Twenty-six analyses with Th/U ratios typical for magmatic zircon (~0.3) give a Concordia age of 1041.6 ± 2.9 Ma (Fig. 8A) that is interpreted as the igneous crystallization age of the granitic protolith. One outlier analysis with a lower age from an U-rich spot was excluded from the age calculation.

4.2.2. Metagabbro (LYD-44-1)

Metagabbro was sampled in a weakly foliated outcrop that is intruded by a subvertical granitic pegmatite sheet (Fig. 7B). The main mineral constituents are blueish-green amphiboles, which have almost completely replaced primary orthopyroxene, and plagioclase. Minor components are biotite, commonly altered to chlorite, and titanite as well as opaque minerals and zircon as accessory phases. Zircon crystals vary in size (up to 300 µm in length) and are subhedral, elongated (aspect ratios 2–5), colorless and transparent. In CL images, they show oscillatory zoning with broad zones parallel to the c-axis that are typical for magmatic zircons from gabbroic melts. Eighteen analyses with Th/U ratios typical for magmatic zircon (0.6–1.05) give a common Concordia age of 1041.3 ± 3.3 Ma (Fig. 8B) that is interpreted as the igneous crystallization age of the gabbro. One reversely discordant outlier analysis has been excluded from the age calculation.

4.2.3. Amphibolite (LYD-35-1)

The sampled amphibolite is intruded by subvertical pinkish pegmatites and contains minor white granitic veins that are concordant with the foliation (Fig. 7C). The sampled rock consists almost entirely of hornblende, plagioclase and minor opaque minerals. Aligned amphiboles and dynamically recrystallized plagioclase form a pronounced L-S-fabric. Zircon occurs as a very rare accessory phase and can be divided into two subpopulations: The first consists of fragments of relatively large, subhedral to anhedral crystals that are colorless and show oscillatory zoning or more complex textures in CL. The second group consists of smaller brownish metamict grains with rounded corners. The comparison with other samples analyzed in this study suggests that the first subpopulation represents the gabbroic protolith and the latter the intrusive granitic veins. Zircons from both populations show thin discontinuous high-luminescent rims and revealed Th/U-ratios in the typical range for magmatic zircon. Analyses from the first zircon population are mostly concordant and give a Concordia age of 1040 ± 11 Ma (Fig. 8C) that is interpreted as the igneous crystallization age of the gabbroic protolith. Metamict zircons from the second subpopulation revealed high U concentrations and generally discordant analyses that define a discordia. The upper intercept age of 1024 ± 10 Ma (Fig. 8C) is interpreted as the crystallization age of the granitic vein that is probably related to the nearby intrusion of granitic pegmatites.

4.2.4. Mylonitic granitic gneiss, mixed series (LYD-169-1)

The sample locality exposes all the different lithologies that constitute the mixed series. The sampled mylonitic gneiss has a leucogranitic composition and is intruded by granite pegmatites with heterogeneous shapes and dimensions. All lithologies in the sampled outcrop are strongly ductilely deformed and folded around moderately E-plunging fold axes. The sampled gneiss has a prominent L-S fabric and consists of finely laminated layers of recrystallized quartz and feldspar and coarser grained pinkish K-feldspar bands, respectively (Fig. 7D). Biotite is the only mafic component and is commonly replaced by chlorite. The analyzed zircons are mostly 100–150 µm in length, brownish, euhedral or subhedral with stubby crystal shapes (aspect ratio ≈ 2) and subrounded corners. In CL images, zircon crystals show oscillatory zoning as well as thin irregular high-luminescent rims. All analyses revealed high U concentrations (800–2000 ppm) and Th/U-ratios typical for magmatic rocks (0.6–1.2). Out of eighteen analyzed grains, four slightly discordant analyses have been excluded to calculate a Concordia age of 1027.1 ± 4.1 Ma (Fig. 8D) that is interpreted as the igneous crystallization age of the granitic protolith.

4.2.5. Mylonitic granitic gneiss, layered gneisses (LYD-83-1)

The sample locality represents the lower limb of a tight, E-plunging fold in mylonitic granitic gneiss with a moderately N-dipping axial surface. Finely laminated layers of recrystallized quartz, feldspar and biotite alternating with coarse-grained pinkish K-feldspar bands (Fig. 7E) constitute the gneissic banding. Elongated rods of quartz and feldspar define an L-S fabric with a shallowly ENE-plunging mineral stretching lineation. The analyzed zircon crystals are slightly brownish, mostly around 100 µm in length, euhedral to subhedral and have stubby shapes (aspect ratio 2–4) with commonly rounded corners. In CL images, most of the zircons show oscillatory zoning typical for magmatic zircons, but also convolute zoning and sector zoning occur. Xenocrystic cores and rims with high U concentrations and diffuse textures are found, but most of the grains have thin discontinuous high-luminescent rims. All of the 22 analyzed spots have Th/U ratios between 0.2–0.4. The oldest and most concordant analyses come from 13 euhedral grains with clear oscillatory zoning and relatively low U (< 400 ppm), and give a Concordia age of 1506.0 ± 4.8 Ma (Fig. 8E) that is interpreted as the igneous crystallization age of the granitic protolith. Rims and diffuse textural domains revealed analyses with high U (400–1600 ppm) that are slightly or strongly discordant and define a Discordia with a lower intercept age of 482 ± 25 Ma, interpreted to reflect metamictization and partial resetting due to a thermal event.

4.2.6. Leucogranite (LYD-163-1)

Gneissic leucogranite (LYD-163-1) was sampled from a 20 m wide, NE–SW-striking, subvertical body that intrudes amphibolite. Inside the body, textures vary diffusively between pegmatitic and medium-grained granite. The sampled rock (Fig. 7F) is mostly equigranular, medium grained and consists of K-feldspar, plagioclase, quartz as well as minor white mica and biotite, which is mostly altered to chlorite.

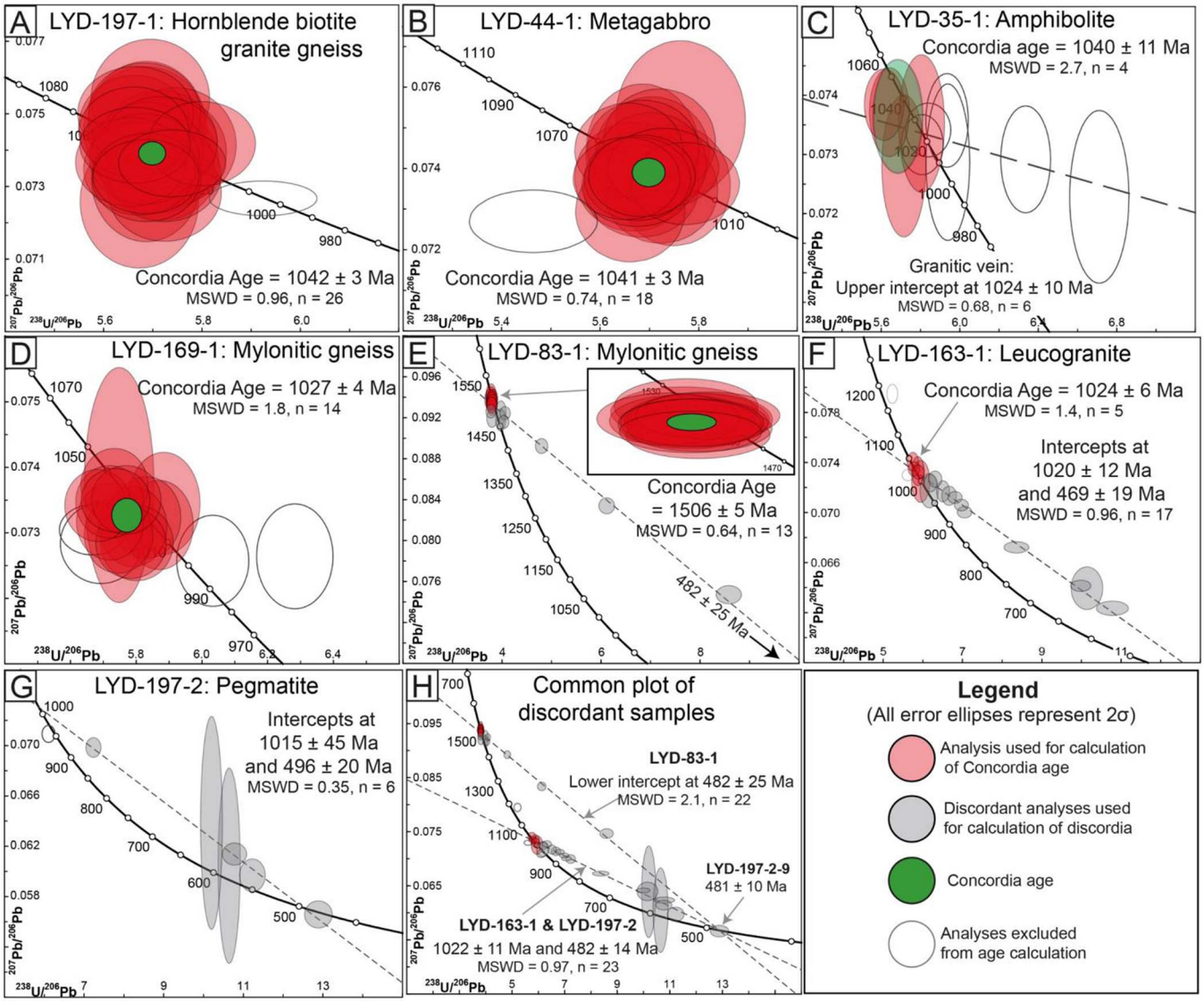

Fig. 8. A–G: Tera-Wasserburg Concordia diagrams of SIMS U–Pb zircon geochronology results. See text for explanation of the age calculations. H: Tera-Wasserburg Concordia diagram of discordant samples LYD-83-1, LYD-163-1 and LYD-197-2. A common Discordia has been calculated for samples LYD-163-1 and LYD-197-2, which represent the same lithological unit. Note that the lower intercept ages from different samples are identical with a concordant analysis from the pegmatite (LYD-197-2).

Quartz and feldspar are partially dynamically recrystallized into a weak L-S-fabric while flame perthites and myrmekites in feldspar appear to represent preserved magmatic textures. The zircon population consists of mostly idiomorphic grains of 100–200 µm in length, which are brown and opaque due to very strong metamictization. Remnants of oscillatory zoning are visible in CL images and some grains exhibit xenocrystic cores, but most internal textures have been obliterated by metamictization. Sixteen analyses of the least metamict grains revealed very high U concentrations reaching up to 4500 ppm and Th/U ratios typical for magmatic zircons (0.4–0.7). The resulting ages show a large scatter along a Discordia line, but a Concordia age of 1024.4 ± 6.3 Ma can be calculated for the most concordant analyses (Fig. 8F) and is interpreted as the igneous crystallization age of the leucogranite. The discordance of U-rich analyses reflects episodic Pb-loss due to thermal resetting and is best constrained by the common lower intercept age of samples LYD-163-1 and LYD-197-2 at 482 ± 14 Ma (Fig. 7H), which represent the same lithological unit. A single older analysis is discordant and most likely represents an inherited core.

4.2.7. Pegmatite (LYD-197-2)

Pegmatite was sampled from a 1 m-wide, subvertical NE–SW-striking dyke that intrudes hornblende biotite granite gneiss (sample LYD-197-1; Fig. 7A). The pegmatite has alkali feldspar granite composition and consists mostly of large pinkish K-feldspar, white plagioclase, grey quartz and subordinate red garnet. Quartz is dynamically recrystallized into elongated rods while large feldspar crystals are only marginally recrystallized and deform mostly by brittle fracturing. The zircon population is characterized by extreme metamictization and consists of brown, non-transparent and commonly idiomorphic crystals, 100–200 µm in length. Due to the extreme metamictization, internal textures are largely obliterated and only eight grains could be analyzed from a large number of picked zircons. All spots revealed very high U concentrations between 1000 and 3500 ppm with Th/U ratios below 0.05. The resulting ages have a large scatter but correlate strongly with U concentrations and define a Discordia line with poorly constrained intercepts at 1015 ± 45 Ma and 496 ± 20 Ma (Fig. 8G). The discordance pattern with one concordant analysis at 481 ± 10 Ma suggests that the strongly metamict grains were partially or completely reset by a thermal event. The pegmatite sample represents the same lithological unit as the leucogranite sample LYD-163-1 and both samples revealed similar zircon populations and resulting ages. Therefore, we assume that the best constraint on the intrusion age of the pegmatite

and the age of the thermal resetting is given by the common discordia line calculated for samples LYD-163-1 and LYD-197-2 together (Fig. 8H) with intercepts at ca. 1022 Ma and 482 Ma, respectively.

4.2.8. Summary of U–Pb zircon geochronology

The oldest rock found in this study is a layer of granitic gneiss (LYD-83-1) with an igneous crystallization age of 1506 ± 5 Ma. The sampled hornblende biotite granite (LYD-197-1) and metagabbro (LYD-44-1) revealed within uncertainties identical crystallization ages of 1042 ± 3 Ma and 1041 ± 3 Ma, which overlap with the crystallization age of the amphibolite (LYD-35-1) at 1040 ± 11 Ma. The granitic protolith of a mylonitic gneiss (LYD-169-1) crystallized at 1027 ± 4 Ma. The intrusion age of gneissic leucogranite (LYD-163-1) is 1024 ± 6 Ma and a related leucogranitic pegmatite (LYD-197-2) is best constrained by a common upper intercept age to ca. 1022 Ma. Three independent samples (LYD-83-1, LYD-163-1 and LYD-197-2) revealed a partial to complete resetting of strongly metamict zircon at ca. 482 Ma.

5. Discussion of U–Pb zircon geochronology

The U–Pb zircon ages acquired in this study range over more than 1000 Ma from ca. 1506 to 482 Ma. The following discussion will show that concordant ages represent the Telemarkian, Sveconorwegian and Caledonian orogenic periods, respectively, but also highlight a major difference between Proterozoic and Paleozoic orogenesis: Proterozoic ages in this dataset represent magmatic activity, while the Caledonian orogeny is only represented by reseting of strongly metamict zircons.

5.1. Magmatic formation history of the eastern Øygarden Complex

The new geochronological data in combination with the results from detailed field mapping allow us to establish the first precise magmatic formation history for the eastern Øygarden Complex. Telemarkian granitoids crystallized at 1506 ± 5 Ma and have lithological compositions resembling the Suldal Arc (Roberts et al., 2013). Sveconorwegian magmatism occurred in two distinct phases; contemporary gabbro and hornblende biotite granite magmatism at ca. 1041 Ma was followed by leucogranitic magmatism in between 1027 ± 4 Ma and ca. 1022 Ma, with leucogranitic pegmatites being the latest intrusives. Field relationships, implying that hornblende biotite granite intruded the gabbro before the latter was entirely crystallized and the observed transition from tonalite to hornblende biotite granite imply a genetic link between gabbroic and granitic magmatism at 1041 Ma. Bimodal magmatism in the eastern Øygarden Complex resembles pre-Sveconorwegian bimodal magmatism in the Telemarkia terrane (Brewer et al., 2004; Spencer et al., 2014). A late- to post-Sveconorwegian (990–920 Ma) Hornblende–Biotite Granite suite in southern Norway might have evolved by extreme magmatic differentiation from mafic magmas (Auwera et al., 2003; Bogaerts et al., 2003), however, contrasting models involve crustal anatexis (c.f. Andersen et al., 2009). In the eastern Øygarden Complex, 1027–1022 Ma leucogranitic magmatism shows a striking contrast in composition to the preceding magmatic phase, yet, it is not clear whether this reflects evolved differentiation of the same parent magma or a different magmatic source.

5.2. Correlating the Øygarden Complex with Telemarkia and the Sirdal magmatic Belt

To constrain the tectonostratigraphic position of the Øygarden Complex, we compared the ages acquired in this study with the occurrence of magmatism in adjacent domains of Baltican basement and Caledonian nappes of continental origin. The two main events dated at around 1500 Ma and 1040 Ma (Fig. 9A) represent distinct magmatic episodes that correspond precisely to the Telemarkian and Sveconorwegian orogenic periods. Igneous rocks of these ages occur in several of the Sveconorwegian domains of southern Norway, but the combination of 1500 Ma and 1040 Ma ages has not been reported from the Caledonian continental nappes (Roffeis and Corfu, 2014). An important finding of this study is that the Øygarden Complex has a distinct Precambrian evolution that is different from that of the WGR. The latter is characterized by Gothian protholiths (1650–1600 Ma) overprinted by late Sveconorwegian (< 1000 Ma) high-grade metamorphism and associated intrusives (e.g. Bingen and Solli, 2009; Roffeis and Corfu, 2014; Rohr et al., 2013; Skår, 2000; Skår et al., 1994; Skår and Pedersen, 2003; Tucker et al., 1987). By contrast, the combination of 1500 Ma and 1040 Ma ages clearly correlates the Øygarden Complex with Telemarkia (Fig. 9A). Furthermore, the newly acquired Sveconorwegian crystallization ages show a precise overlap with emplacement ages of the Sirdal Magmatic Belt in southern Norway (Fig. 9B). Ages of Sirdal Magmatic Belt granites form two clusters around 1050 and 1030 Ma (Coint et al., 2015) which resemble two distinct magmatic phases recorded in the eastern Øygarden Complex around 1040 Ma and 1027–1022 Ma. Nevertheless, it is interesting to note that 1040 Ma bimodal magmatism in the Øygarden Complex falls within a period of relatively low magmatic activity in the Sirdal Magmatic Belt (Fig. 9B). Both areas have a number of common features, such as leucogranites with diffuse textural variations and xenolith-rich zones (Mixed Series in the eastern Øygarden Complex). Large parts of the Sirdal Magmatic Belt are virtually undeformed (Slagstad et al., 2013a), in contrast to the strong deformation that overprinted the eastern Øygarden Complex. Yet we argue, that the ductile deformation described in this study is entirely Caledonian (see section 6 for discussion), highlighting the absence of Sveconorwegian deformation as an important similarity between the Øygarden Complex and the Sirdal Magmatic Belt. Our results suggest that the Øygarden Complex is part of the Telemarkia domain of the autochthonous Baltican basement that has been subject to strong Caledonian deformation. Based on similar ages and the geographic relationship between the two areas (Fig. 9C), we furthermore propose that the Øygarden Complex represents a northern, “caledonized” continuation of the Sirdal Magmatic Belt.

5.3. Implications for Sveconorwegian orogeny in SW Norway and reconstructions of the pre-Caledonian architecture of the Baltican margin

The newly acquired Sveconorwegian ages from the eastern Øygarden Complex are very relevant with respect to the lively debate about the style of the Sveconorwegian orogeny. The contemporaneous occurrence of gabbroic and granitic magmatism at 1041 Ma found in this study, is more in accordance with arc-magmatism in an accretionary setting (Slagstad et al., 2013a) than with syn-collisional magmatism caused by crustal thickening (Bingen et al., 2008b). Furthermore, we found no record of Sveconorwegian high-grade metamorphism or deformation in the eastern Øygarden Complex. This is consistent with interpretations of the Sirdal Magmatic Belt in the context of an accretionary Sveconorwegian orogen (Coint et al., 2015; Slagstad et al., 2013a). Based on findings from the Caledonian Hardanger-Ryfylke Nappe Complex, Roffeis et al. (2013) argue that Gothian rocks were thrust on top of Telemarkian rocks around 1000 Ma, but it is not clear where this tectonism took place and whether it represents accretion or continental collision. As large parts of the pre-Caledonian basement in southern Norway remain poorly studied, we believe that the spatiotemporal evolution of the Sveconorwegian orogeny, which spans more than 200 m.y. (Bingen et al., 2008b), could be more complex than hitherto resolved by available data. In the light of our results, however, we favor an accretionary model (Slagstad et al., 2017). Clockwise rotation and soft collision of Baltica’s southern margin with Amazonia is an alternative scenario that cannot be ruled out based on presently available data (Cawood and Pisarevsky, 2017).

Our finding of Telemarkian crust in the Øygarden Complex and its interpretation as a northern continuation of the Sirdal Magmatic Belt contradicts the orientation and location of previously proposed terrane

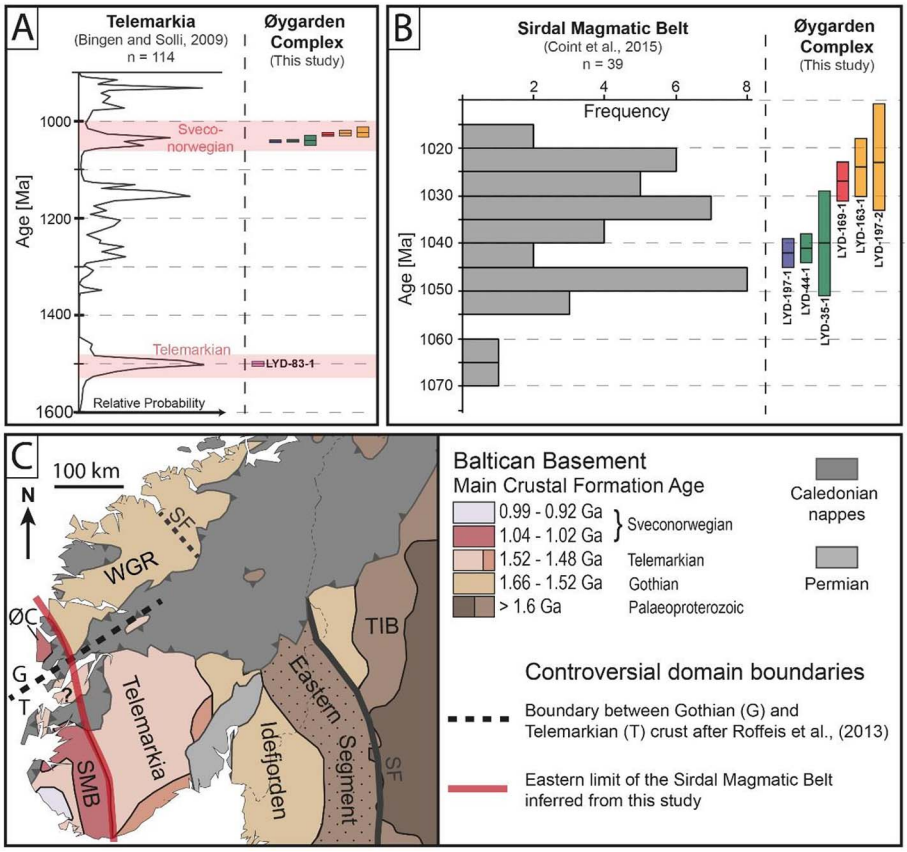

Fig. 9. A: Comparison of magmatic ages from this study with the relative probability of magmatic ages in the Telemarkia domain (Bingen and Solli, 2009). Error bars represent 2σ and colors correspond to the legend in Fig. 3. B: Comparison of Sveconorwegian igneous ages from this study and the Sirdal Magmatic Belt (Coint et al., 2015). Error bars represent 2σ and colors correspond to the legend in Fig. 3. C: Schematic map proposing the Øygarden Complex (ØC) as a northern continuation of the Sirdal Magmatic Belt (SMB). The suggested NNW-trending domain boundary highlights the difference between Øygarden Complex and Western Gneiss Region (WGR) and contradicts the inferred border of Gothian and Telemarkian crust proposed by Roffeis et al. (2013).

boundaries in SW Norway (Fig. 9C). Roffeis et al. (2013) and Roffeis and Corfu (2014) suggested a ENE–WSW-trending terrane boundary to explain different ages of the crust in Telemarkia (< 1.52 Ga) and the Gothian crust (1.66–1.52 Ga) in the WGR. In contrast, our interpretation of a continuous NNW-trend of Sveconorwegian domain boundaries into the 'caledonized' part of the Baltican basement is consistent with the NW-trending limit of Sveconorwegian overprint in the WGR (Bingen et al., 2008a) and the general strike of domain boundaries in the entire Sveconorwegian province (Fig. 9C). The distinction between Øygarden Complex and WGR found in this study suggests that the northern branch of the Bergen Arc Shear Zone separates different crustal domains (Fig. 2). Possibly, this crustal lineament originated during the Sveconorwegian orogeny and was later reactivated by post-Caledonian extensional deformation (Wennberg et al., 1998). Even though we reject the reconstruction of the pre-Caledonian architecture proposed by Roffeis et al. (2013), we agree that the obvious difference in crustal formation ages between the WGR and Telemarkia (including Øygarden Complex) needs to be explained. In our opinion, the relation between these domains is still an open question with great significance for the Sveconorwegian crustal assembly of Baltica as well as Caledonian tectonic reconstructions.

5.4. Significance of the early Ordovician (482 Ma) lower intercept age

None of the three samples with discordant zircon data (LYD-83-1, LYD-163-1 & LYD-197-2) revealed zircon textures that could relate the lower intercept ages to metamorphic recrystallization. The discordant analyses are associated with idiomorphic magmatic zircons with very high U concentrations. In these samples, a strong correlation between U concentration and resulting age is observed. The most discordant analyses and youngest ages come from the highly radioactive leucogranite and pegmatite samples that are the least deformed of the analyzed samples. The samples that show the strongest state of dynamic recrystallization at amphibolite and greenschist facies conditions (LYD-35-1, LYD-83-1 & LYD-169-1) revealed zircons with thin discontinuous U-poor rims, which were too thin to analyze. Therefore, we interpret the ca. 482 Ma lower intercept age as a partial to complete resetting of metamict grains caused by a rapid temperature increase from low temperatures to above the 'critical amorphization temperature' of ~360 °C, as demonstrated by diffusion experiments (Cherniak and Watson, 2003). The intense ductile deformation of the eastern Øygarden Complex related to a regional amphibolite facies metamorphic event might be recorded in the thin U-poor rims, but their age was not determined. In our geochronological dataset, the early Ordovician (ca. 482 Ma) resetting of strongly metamict zircons is the only record of the entire Caledonian orogenic cycle. This result seems surprising only at first sight, as it actually reflects the typical behavior of the U–Pb zircon system with its robustness to high temperatures and vulnerability to diffusional Pb-loss at low temperatures because of metamictization (Mezger and Krogstad, 1997). Residence at low temperatures over several hundred million years is necessary for U-rich grains to accumulate enough metamictization to allow the strong or complete resetting through Pb-diffusion that is recorded in our dataset (Cherniak and Watson, 2003). Thus, this part of the Baltoscandian platform must have been exhumed soon after the Sveconorwegian orogeny and resided at shallow crustal levels through most of the Neoproterozoic and early Paleozoic. This thermal history likely reflects the Cryogenian to Cambrian rift to drift history of Baltica related to the break-up of Rodinia and the opening of the Iapetus Ocean (Abdelmalak et al., 2015; Andersen et al., 2012; Gee et al., 2017; Torsvik et al., 1996). The suggested temperature increase in the Øygarden Complex at 482 Ma, on the other hand, falls into the poorly understood early Caledonian period. Early Ordovician ages of magmatism and metamorphism are very common in the Upper Allochthon of the Caledonian orogenic wedge. They imply considerable tectonic activity in the early Ordovician in outboard terranes and at the Laurentian margin (e.g.

Corfu et al., 2014; Dunning and Pedersen, 1988; Gee et al., 2013; Hacker and Gans, 2005; Klonowska et al., 2014; Pedersen et al., 1992; Pedersen and Dunning, 1997; Root and Corfu, 2012; Slagstad et al., 2014). In contrast, early Ordovician ages have not yet been reported from rocks that are clearly part of the autochthonous Baltican basement, as is the case with the eastern Øygarden Complex, although Ordovician intrusive rocks are intricately folded into the basement gneisses of the northern WGR (e.g. Tucker et al., 2004). Recently, Jakob et al. (2017) presented new evidence for early Ordovician magmatic activity in the Samnanger mélange, which rests now in the Caledonian nappe pile above the Øygarden Complex (Fig. 2). These authors interpret the mélange to represent the Pre-Caledonian hyperextended margin of Baltica and suggest two possible tectonic scenarios for the early Ordovician: 1. The hyperextended margin formed in the Ediacaran and experienced latest Cambrian–early Ordovician tectonomagmatic activity related to shortening of transitional crust. 2. The mélange formed entirely through latest Cambrian–early Ordovician (back-arc) extension. In an alternative model, Slama and Pedersen (2015) argue that the mélange represents an Ordovician arc located in between Baltica and an outboard microcontinent. Our results cannot confirm or contradict any of these models. However, they show that Ordovician tectonothermal activity seems to have affected the proximal domain of the Baltican margin, as represented by the Øygarden Complex. Furthermore, this thermal event seems to have been strong enough to anneal metamictization completely, as no Pb-loss occurred during subsequent Scandian metamorphism.

6. Caledonian tectonic evolution of the eastern Øygarden Complex

As previously discussed (section 5.1), U–Pb zircon geochronology could not constrain the timing of the ductile reworking of the eastern Øygarden Complex. In the context of regional geologic models, however, this deformation must have occurred during the Caledonian orogenic cycle (e.g. Fossen and Dunlap, 1998; Johns, 1981; Rykkelid and Fossen, 1992). Structural analysis showed a geometric relationship between all fabrics and structures with consistent fabric orientations indifferent of metamorphic grade, including widespread low-grade deformation. We have not identified distinct fabrics that could represent a Precambrian deformation history. Previous thermochronological studies in the western Øygarden Complex found early Devonian ages for amphibolite facies metamorphism and subsequent cooling to the brittle-ductile transition (Boundy et al., 1996; Fossen and Dunlap, 1998; Larsen et al., 2003). These ages represent the best available constraints on the timing of ductile reworking in the eastern Øygarden Complex, as they correspond well to the metamorphic sequence found in this study. Yet, the absence of top-to-W kinematics and the abundance of ductile-to-brittle top-to-E low-angle shear zones with intensive low-grade deformation in the eastern Øygarden Complex require further discussion. There are two plausible scenarios that could explain the absence of top-to-W deformation: (I) the eastern Øygarden Complex and the basal contact of the nappes comprise a large tectonic lens that escaped post-orogenic top-to-W shearing and preserves Scandian contractional deformation. (II) At least to some degree, the top-to-E deformation in the eastern Øygarden Complex is also extensional (post-orogenic). As extensional top-to-W shearing affected structurally lower levels, the latter case would imply bi-directional extension in the Øygarden Complex.

Since precise thermochronological constraints on the age of the deformation are lacking, it is difficult to distinguish between contractional and extensional deformation. However, the ENE-plunge of linear fabrics in the eastern Øygarden Complex, is slightly oblique to the regional direction of Scandian thrusting (e.g. Fossen, 2000). Furthermore, the occurrence of constrictional fabrics as well as the abundance of lineation-parallel folds seem to be structurally better compatible with a Devonian transtensional system (Fossen et al., 2013; Krabbendam and Dewey, 1998; Osmundsen and Andersen, 2001) than with Scandian thrusting. More importantly, however, the progressive overprinting of brittle structures on previously ductile fabrics in low-angle shear zones with top-to-E kinematics, such as the Loddefjord shear zone, records exhumation during shearing. The phyllonites that formed in these shear zones are comparable to similar fault rocks in the Nordfjord Sogn detachment zone and have arguably an extraordinarily low shear strength (Braathen et al., 2004). If one assumes that these phyllonitic top-to-E fabrics formed during Scandian thrusting, they should have become overprinted by the intense extensional top-to-W deformation that overprinted gneisses with similar fabric orientation nearby (Rykkelid and Fossen, 1992). This implies that the phyllonitic top-to-E shear zones presumably formed during post-orogenic extension. Based on the identical orientation of amphibolite and upper greenschist facies fabrics it cannot be ruled out that also higher-grade mylonitic top-to-E deformation could have been extensional. Comparing the structure of the Øygarden Complex with similar basement windows in the central Norwegian Caledonides (Braathen et al., 2000; Osmundsen et al., 2005), we speculate that the Øygarden Complex could represent an early Devonian core complex. We believe that such a model could explain the occurrence of opposed shear-senses within the mylonitic foliation, constrictional fabrics with lineation parallel folds as well as low-angle normal-sense shear zones recording fluid-related strain weakening facilitating deformation at the brittle-ductile transition (Whitney et al., 2013).

7. Summary and conclusions

The evolution of continental crust in the eastern Øygarden Complex through three distinct orogenic periods as well as intermittent episodes of extension and tectonic quiescence is summarized in Fig. 10.

- The eastern Øygarden Complex consists of Telemarkian (1506 ± 5 Ma) granitic basement that was intruded by voluminous Sveconorwegian melts. These Grenville-age rocks formed through two distinct magmatic events: Bimodal gabbro and hornblende biotite granite magmatism at ca. 1041 Ma was followed by leucogranitic magmatism at ca. 1027–1022 Ma.
- The Precambrian evolution of the Øygarden Complex is distinct from that of the WGR. The Øygarden Complex rather represents a part of Telemarkia and a northern continuation of the Sirdal Magmatic Belt, but with a strong Caledonian overprint. Our results contradict previously proposed terrane boundaries (Roffeis and Corfu, 2014; Roffeis et al., 2013) separating Gothian and Telemarkian crust.
- Careful ion microprobe dating did not reveal any record of Sveconorwegian tectono-metamorphism in the eastern Øygarden Complex. In accordance with the undeformed Sirdal Magmatic Belt further south, our results support an accretionary Sveconorwegian orogen (e.g. Slagstad et al., 2013a), rather than involvement in a major continent-continent collision in the period 1040–1020 Ma.
- Resetting of strongly metamict zircons at ca. 482 Ma indicates an early Ordovician thermal event, reflecting either extension of the Baltican margin or early Caledonian convergence. Scandian regional metamorphism left no measurable record in the U-Pb zircon system.
- Caledonian ductile reworking involved east-directed shearing and recumbent lineation-parallel folding, followed by the formation of ductile-to-brittle top-to-E shear zones. Whether these E-directed fabrics/structures relate to Caledonian thrusting or post-Caledonian extension needs to be resolved by careful thermochronological dating. However, based on field observations, we currently favor an extensional origin related to the exhumation of the Øygarden Complex, possibly as an early Devonian core complex.

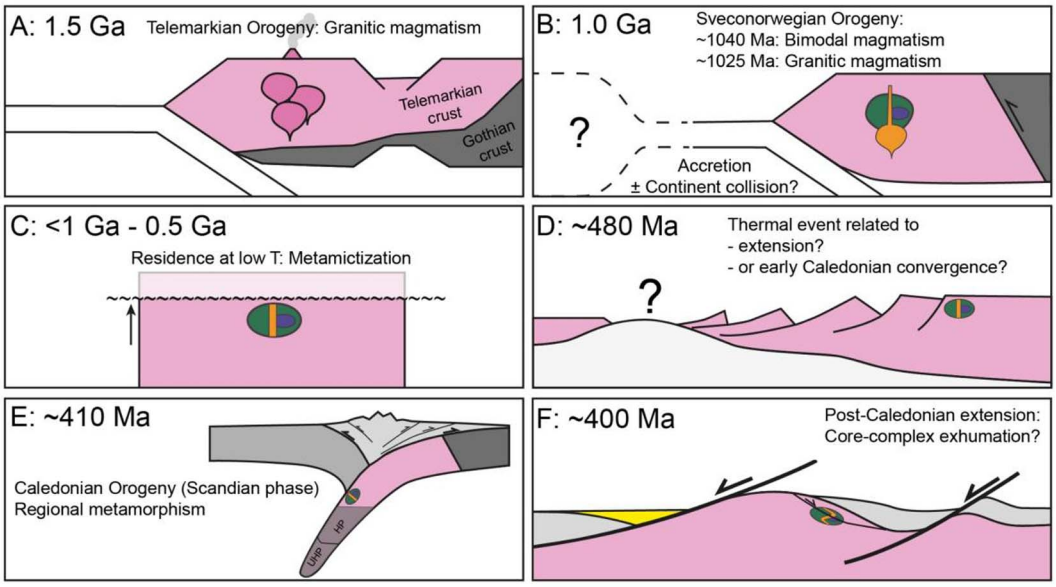

Fig. 10. Cartoon illustrating the geologic evolution of the eastern Øygarden Complex from the Mesoproterozoic to the early Devonian. Note that the colors correspond to the map units in Fig. 3. A, B are modified from (Roberts and Slagstad (2015)). D is based on (Andersen et al., 2012). E, F are modified from Fossen et al. (2017).

Acknowledgements

We thank Irina Dumitru, Martina Suppersberger Hamre, Egil Erichsen and Irene Heggstad at UiB for help with sample preparation and CL imaging. Martin Whitehouse, Lev Ilinsky and Kerstin Lindén at NordSIMS, Stockholm are thanked for great help with geochronology. We thank Fernando Corfu and one anonymous reviewer for thorough reviews that helped to improve the manuscript. JDW was supported by a DAAD student grant; and VISTA – a basic research program in collaboration between The Norwegian Academy of Science and Letters, and Statoil [grant number 6271]. The NordSIMS facility is supported by the research funding agencies of Denmark, Iceland, Norway and Sweden, and the Swedish Museum of Natural History. This is NordSIMS contribution number 534.

Appendix A. Supplementary data

Supplementary data associated with this article can be found, in the online version, at http://dx.doi.org/10.1016/j.precamres.2017.11.020.

References

Abdelmalak, M.M., Andersen, T.B., Planke, S., Faleide, J.I., Corfu, F., Tegner, C., Shephard, G.E., Zastrozhnov, D., Myklebust, R., 2015. The ocean-continent transition in the mid-Norwegian margin: insight from seismic data and an onshore Caledonian field analogue. Geology 43, 1011–1014. http://dx.doi.org/10.1130/G37086.1.

Allmendinger, R.W., Cardozo, N., Fisher, D.M., 2011. Structural Geology Algorithms: Vectors and Tensors. Cambridge University Press, Cambridge, pp. 302.

Andersen, T.B., Jamtveit, B., 1990. Uplift of deep crust during orogenic extensional collapse – a model based on field studies in the Sogn-Sunnfjord Region of Western Norway. Tectonics 9, 1097–1111. http://dx.doi.org/10.1029/TC009i005p01097.

Andersen, T.B., Jamtveit, B., Dewey, J.F., Swensson, E., 1991. Subduction and eduction of continental-crust – major mechanisms during continent-continent collision and orogenic extensional collapse, a model based on the South Norwegian Caledonides. Terra Nova 3, 303–310. http://dx.doi.org/10.1111/j.1365-3121.1991.tb00148.x.

Andersen, T., Graham, S., Sylvester, A.G., 2009. The geochemistry, Lu–Hf isotope systematics, and petrogenesis of Late Mesoproterozoic A-type granites in southwestern Fennoscandia. Can. Mineral. 47, 1399–1422. http://dx.doi.org/10.3749/canmin.47.6.1399.

Andersen, T.B., Corfu, F., Labrousse, L., Osmundsen, P.T., 2012. Evidence for hyperextension along the pre-Caledonian margin of Baltica. J. Geol. Soc. 169, 601–612. http://dx.doi.org/10.1144/0016-76492012-011.

Andresen, A., Steltenpohl, M.G., 1994. Evidence for ophiolite obduction, terrane accretion and polyorogenic evolution of the north Scandinavian Caledonides. Tectonophysics 231, 59–70. http://dx.doi.org/10.1016/0040-1951(94)90121-X.

Askvik, H., 1971. Gabbroic and Quartz Dioritic Intrusions in Gneisses on Southern Askoy, West Norwegian Caledonides. Norges Geologiske Undersøkelse 270, 3–38.

Augland, L.E., Andresen, A., Gasser, D., Steltenpohl, M.G., 2014. Early Ordovician to Silurian evolution of exotic terranes in the Scandinavian Caledonides of the Ofoten-Troms area – terrane characterization and correlation based on new U-Pb zircon ages and Lu–Hf isotopic data. Geol. Soc. London Spec. Publ. 390, 655–678. http://dx.doi.org/10.1144/sp390.19.

Auwera, J.V., Bogaerts, M., Liégeois, J.-P., Demaiffe, D., Wilmart, E., Bolle, O., Duchesne, J.C., 2003. Derivation of the 1.0–0.9 Ga ferro-potassic A-type granitoids of southern Norway by extreme differentiation from basic magmas. Precambr. Res. 124, 107–148. http://dx.doi.org/10.1016/S0301-9268(03)00084-6.

Bering, D.H., 1985. Tektonometamorf Utvikling Av Det Vestlige Gneiskompleks I Sund. University of Bergen, Sotra, pp. 367.

Bingen, B., Solli, A., 2009. Geochronology of magmatism in the Caledonian and Sveconorwegian belts of Baltica: synopsis for detrital zircon provenance studies. Norw. J. Geol. 89, 267–290.

Bingen, B., Van Breemen, O., 1998. Tectonic regimes and terrane boundaries in the high-grade Sveconorwegian belt of SW Norway, inferred from U-Pb zircon geochronology and geochemical signature of augen gneiss suites. J. Geol. Soc. 155, 143–154. http://dx.doi.org/10.1144/gsjgs.155.1.0143.

Bingen, B., Demaiffe, D., Hertogen, J., Weis, D., Michot, J., 1993. K-rich calc-alkaline Augen Gneisses of Grenvillian age in Sw Norway – mingling of mantle-derived and crustal components. J. Geol. 101, 763–778.

Bingen, B., Skar, O., Marker, M., Sigmond, E.M.O., Nordgulen, O., Ragnhildstveit, J., Mansfeld, J., Tucker, R.D., Liegeois, J.P., 2005. Timing of continental building in the Sveconorwegian orogen, SW Scandinavia. Norw. J. Geol. 85, 87–116.

Bingen, B., Davis, W.J., Hamilton, M.A., Engvik, A.K., Stein, H.J., Skar, O., Nordgulen, O., 2008a. Geochronology of high-grade metamorphism in the Sveconorwegian belt, S. Norway: U-Pb, Th-Pb and Re-Os data. Norw. J. Geol. 88, 13–42.

Bingen, B., Nordgulen, O., Viola, G., 2008b. A four-phase model for the Sveconorwegian orogeny, SW Scandinavia. Norw. J. Geol. 88, 43–72.

Bogaerts, M., Scaillet, B., Liégeois, J.-P., Vander Auwera, J., 2003. Petrology and geochemistry of the Lyngdal granodiorite (Southern Norway) and the role of fractional crystallisation in the genesis of Proterozoic ferro-potassic A-type granites. Precambr. Res. 124, 149–184. http://dx.doi.org/10.1016/S0301-9268(03)00085-8.

Bos, B., Spiers, C.J., 2002. Frictional-viscous flow of phyllosilicate-bearing fault rock: microphysical model and implications for crustal strength profiles. J. Geophys. Res. Solid Earth 107http://dx.doi.org/10.1029/2001jb000301. ECV 1-1-ECV 1-13.

Boundy, T.M., Essene, E.J., Hall, C.M., Austrheim, H., Halliday, A.N., 1996. Rapid exhumation of lower crust during continent-continent collision and late extension: evidence from Ar-40/Ar-39 incremental heating of hornblendes and muscovites, Caledonian orogen, western Norway. Geol. Soc. Am. Bull. 108, 1425–1437. http://dx.doi.org/10.1130/0016-7606(1996) 108.

Braathen, A., Nordgulen, O., Osmundsen, P.T., Andersen, T.B., Solli, A., Roberts, D., 2000. Devonian, orogen-parallel, opposed extension in the Central Norwegian Caledonides. Geology 28, 615–618. http://dx.doi.org/10.1130/0091-7613(2000) 28.

Braathen, A., Osmundsen, P.T., Gabrielsen, R.H., 2004. Dynamic development of fault rocks in a crustal-scale detachment: an example from western Norway. Tectonics 23. http://dx.doi.org/10.1029/2003tc001558.

Brewer, T.S., Åhäll, K.I., Menuge, J.F., Storey, C.D., Parrish, R.R., 2004. Mesoproterozoic bimodal volcanism in SW Norway, evidence for recurring pre-Sveconorwegian continental margin tectonism. Precambr. Res. 134, 249–273. http://dx.doi.org/10.1016/j.precamres.2004.06.003.

Brueckner, H.K., Van Roermund, H.L.M., Pearson, N.J., 2004. An archean(?) to paleozoic evolution for a garnet peridotite lens with sub-baltic shield affinity within the Seve Nappe Complex of Jamtland, Sweden, central Scandinavian Caledonides. J. Petrol.

45, 415–437. http://dx.doi.org/10.1093/petrology/egg088.
Bybee, G.M., Ashwal, L.D., Shirey, S.B., Horan, M., Mock, T., Andersen, T.B., 2014. Pyroxene megacrysts in Proterozoic anorthosites: implications for tectonic setting, magma source and magmatic processes at the Moho. Earth Planet. Sci. Lett. 389, 74–85. http://dx.doi.org/10.1016/j.epsl.2013.12.015.
Cawood, P.A., Pisarevsky, S.A., 2017. Laurentia-Baltica-Amazonia relations during Rodinia assembly. Precambr. Res. 292, 386–397. http://dx.doi.org/10.1016/j.precamres.2017.01.031.
Chauvet, A., Seranne, M., 1994. Extension-parallel folding in the Scandinavian Caledonides – implications for Late-Orogenic processes. Tectonophysics 238, 31–54. http://dx.doi.org/10.1016/0040-1951(94)90048-5.
Cherniak, D.J., Watson, E.B., 2003. Diffusion in zircon. Rev. Mineral. Geochem. 53, 113–143. http://dx.doi.org/10.2113/0530113.
Cocks, L.R.M., Torsvik, T.H., 2005. Baltica from the late Precambrian to mid-Palaeozoic times: the gain and loss of a terrane's identity. Earth Sci. Rev. 72, 39–66. http://dx.doi.org/10.1016/j.earscirev.2005.04.001.
Coint, N., Slagstad, T., Roberts, N.M.W., Marker, M., Rohr, T., Sorensen, B.E., 2015. The Late Mesoproterozoic Sirdal Magmatic Belt, SW Norway: relationships between magmatism and metamorphism and implications for Sveconorwegian orogenesis. Precambr. Res. 265, 57–77. http://dx.doi.org/10.1016/j.precamres.2015.05.002.
Corfu, F., Hanchar, J.M., Hoskin, P.W., Kinny, P., 2003. Atlas of zircon textures. Rev. Mineral. Geochem. 53, 469–500. http://dx.doi.org/10.2113/0530469.
Corfu, F., Andersen, T., Gasser, D., 2014. The Scandinavian Caledonides: main features, conceptual advances and critical questions. Geol. Soc. London Spec. Publ. 390, 9–43. http://dx.doi.org/10.1144/SP390.25.
Dunning, G.R., Pedersen, R.B., 1988. U/Pb ages of ophiolites and arc-related plutons of the Norwegian Caledonides – implications for the development of Iapetus. Contrib. Miner. Petrol. 98, 13–23. http://dx.doi.org/10.1007/Bf00371904.
Eide, E.A., Torsvik, T.H., Andersen, T.B., 1997. Absolute dating of brittle fault movements: Late Permian and late Jurassic extensional fault breccias in western Norway. Terra Nova 9, 135–139.
Essex, R.M., Gromet, L.P., Andreasson, P.G., Albrecht, L., 1997. Early Ordovician U-Pb metamorphic ages of the eclogite-bearing Seve Nappes, northern Scandinavian Caledonides. J. Metamorph. Geol. 15, 665–676. http://dx.doi.org/10.1111/j.1525-1314.1997.00048.x.
Faerseth, R.B., Gjelberg, J., Martinsen, O.J., 2011. Structural geology and sedimentology of Silurian metasediments in the Ulven area, Major Bergen Arc, SW Norway. Norw. J. Geol. 91, 19–33.
Fossen, H., 1989. Geology of the minor Bergen arc, West Norway. Norges Geologiske Undersøkelse Bull. 416, 47–62.
Fossen, H., 1992. The role of extensional tectonics in the Caledonides of South Norway. J. Struct. Geol. 14, 1033–1046. http://dx.doi.org/10.1016/0191-8141(92)90034-T.
Fossen, H., 1993. Linear fabrics in the bergsdalen nappes, southwest Norway – implications for deformation history and fold development. Nor. Geol. Tidsskr. 73, 95–108.
Fossen, H., 1998. Advances in understanding the post-Caledonian structural evolution of the Bergen Area, West Norway. Nor. Geol. Tidsskr. 78, 33–46.
Fossen, H., 2000. Extensional tectonics in the Caledonides: synorogenic or postorogenic? Tectonics 19, 213–224. http://dx.doi.org/10.1029/1999tc900066.
Fossen, H., 2010. Extensional tectonics in the North Atlantic Caledonides: a regional view. Geol. Soc. London Spec. Publ. 335, 767–793. http://dx.doi.org/10.1144/SP335.31.
Fossen, H., Dunlap, W.J., 1998. Timing and kinematics of Caledonian thrusting and extensional collapse, southern Norway: evidence from Ar-40/Ar-39 thermochronology. J. Struct. Geol. 20, 765–781. http://dx.doi.org/10.1016/S0191-8141(98)00007-8.
Fossen, H., Dunlap, W.J., 2006. Age constraints on the late Caledonian (Scandian) deformation in the major Bergen Arc, SW Norway. Norw. J. Geol. 86, 59–70.
Fossen, H., Hurich, C.A., 2005. The Hardangerfjord Shear Zone in SW Norway and the North Sea: a large-scale low-angle Shear Zone in the Caledonian crust. J. Geol. Soc. 162, 675–687. http://dx.doi.org/10.1144/0016-764904-136.
Fossen, H., Rykkelid, E., 1990. Shear zone structures in the Oygarden Area, West Norway. Tectonophysics 174, 385–397. http://dx.doi.org/10.1016/0040-1951(90)90333-4.
Fossen, H., Rykkelid, E., 1992a. The Interaction between oblique and layer-parallel shear in high-strain zones – observations and experiments. Tectonophysics 207, 331–343. http://dx.doi.org/10.1016/0040-1951(92)90394-L.
Fossen, H., Rykkelid, E., 1992b. Postcollisional extension of the caledonide orogen in Scandinavia – structural expressions and tectonic significance. Geology 20, 737–740. http://dx.doi.org/10.1130/0091-7613(1992) 020∗0737:Peotco>2.3.Co;2.
Fossen, H., Teyssier, C., Whitney, D.L., 2013. Transtensional folding. J. Struct. Geol. 56, 89–102. http://dx.doi.org/10.1016/j.jsg.2013.09.004.
Fossen, H., Khani, H.F., Faleide, J.I., Ksienzyk, A.K., Dunlap, W.J., 2016. Post-Caledonian extension in the West Norway–northern North Sea region: the role of structural inheritance. Geol. Soc. London Spec. Publ. 439. http://dx.doi.org/10.1144/SP439.6.
Fossen, H., Cavalcante, G.C., de Almeida, R.P., 2017. Hot versus cold orogenic behavior: comparing the araçuaí-West Congo and the Caledonian Orogens. Tectonics. http://dx.doi.org/10.1002/2017TC004743. n/a–n/a.
Furnes, H., Dilek, Y., Pedersen, R.B., 2012. Structure, geochemistry, and tectonic evolution of trench-distal backarc oceanic crust in the western Norwegian Caledonides, Solund-Stavfjord ophiolite (Norway). Geol. Soc. Am. Bull. 124, 1027–1047. http://dx.doi.org/10.1130/B30561.1.
Gee, D.G., 1975. A tectonic model for the central part of the Scandinavian Caledonides. Am. J. Sci. A275, 468–515.
Gee, D.G., Fossen, H., Henriksen, N., Higgins, A.K., 2008. From the early Paleozoic platforms of Baltica and Laurentia to the Caledonide orogen of Scandinavia and Greenland. Episodes 31, 44–51.
Gee, D.G., Janak, M., Majka, J., Robinson, P., van Roermund, H., 2013. Subduction along and within the Baltoscandian margin during closing of the Iapetus Ocean and Baltica-Laurentia collision. Lithosphere 5, 169–178. http://dx.doi.org/10.1130/L220.1.
Gee, D.G., Andréasson, P.-G., Li, Y., Krill, A., 2017. Baltoscandian margin, Sveconorwegian crust lost by subduction during Caledonian collisional orogeny. GFF 139, 36–51. http://dx.doi.org/10.1080/11035897.2016.1200667.
Gordon, S.M., Whitney, D.L., Teyssier, C., Fossen, H., 2013. U-Pb dates and trace-element geochemistry of zircon from migmatite, Western Gneiss Region, Norway: significance for history of partial melting in continental subduction. Lithos 170, 35–53. http://dx.doi.org/10.1016/j.lithos.2013.02.003.
Hacker, B.R., Gans, P.B., 2005. Continental collisions and the creation of ultrahigh-pressure terranes: petrology and thermochronology of nappes in the central Scandinavian Caledonides. Geol. Soc. Am. Bull. 117, 117–134. http://dx.doi.org/10.1130/B25549.1.
Hacker, B.R., Andersen, T.B., Johnston, S., Kylander-Clark, A.R.C., Peterman, E.M., Walsh, E.O., Young, D., 2010. High-temperature deformation during continental-margin subduction & exhumation: the ultrahigh-pressure Western Gneiss Region of Norway. Tectonophysics 480, 149–171. http://dx.doi.org/10.1016/j.tecto.2009.08.012.
Jakob, J., Alsaif, M., Corfu, F., Andersen, T.B., 2017. Age and origin of thin discontinuous gneiss sheets in the distal domain of the magma-poor hyperextended pre-Caledonian margin of Baltica, southern Norway. J. Geol. Soc. http://dx.doi.org/10.1144/jgs2016-049.
Jeon, H., Whitehouse, M.J., 2015. A critical evaluation of U-Pb calibration schemes used in SIMS zircon geochronology. Geostand. Geoanal. Res. 39, 443–452. http://dx.doi.org/10.1111/j.1751-908X.2014.00325.x.
Johns, C.C., 1981. The Geology of Northern Sotra: Precambrian Gneisses West of the Bergen Arcs. University of London, Norway, Bedford College, pp. 397.
Johnston, S., Hacker, B.R., Ducea, M.N., 2007. Exhumation of ultrahigh-pressure rocks beneath the Hornelen segment of the Nordfjord-Sogn Detachment Zone, western Norway. Geol. Soc. Am. Bull. 119, 1232–1248. http://dx.doi.org/10.1130/B26172.1.
Klonowska, I., Majka, J., Janák, M., Gee, D.G., Ladenberger, A., 2014. Pressure–temperature evolution of a kyanite–garnet pelitic gneiss from Åreskutan: evidence of ultra-high-pressure metamorphism of the Seve Nappe Complex, west-central Jämtland, Swedish Caledonides. Geol. Soc. London Spec. Publ. 390, 321–336. http://dx.doi.org/10.1144/SP390.7.
Knudsen, T.L., Fossen, H., 2001. The Late Jurassic Bjoroy Formation: a provenance indicator for offshore sediments derived from SW Norway as based on single zircon (SIMS) data. Nor. Geol. Tidsskr. 81, 283–292.
Kolderup, C.F., Kolderup, N.H., 1940. Geology of the Bergen Arc System. Bergen Museums Skrifter 20, 137.
Krabbendam, M., Dewey, J.F., 1998. Exhumation of UHP rocks by transtension in the Western Gneiss Region, Scandinavian Caledonides. Geol. Soc. London Spec. Publ. 135, 159–181.
Ksienzyk, A.K., Dunkl, I., Jacobs, J., Fossen, H., Kohlmann, F., 2014. From orogen to passive margin: constraints from fission track and (U–Th)/He analyses on Mesozoic uplift and fault reactivation in SW Norway. Geol. Soc. London Spec. Publ. 390, 679–702. http://dx.doi.org/10.1144/SP390.27.
Ksienzyk, A.K., Wemmer, K., Jacobs, J., Fossen, H., Schomberg, A.C., Sussenberger, A., Lunsdorf, N.K., Bastesen, E., 2016. Post-Caledonian brittle deformation in the Bergen area, West Norway: results from K-Ar illite fault gouge dating. Norw. J. Geol. 96, 275–299. https://doi.org/10.17850/njg96-3-06.
Kvale, A., 1960. The nappe area of the Caledonides in western Norway. Norges Geologiske Undersøkelse Bull. 21–43 212e.
Larsen, O., 1996. Fedjedomens tektoniske utvikling (Øygarden gneiskompleks, vest Norge) – en alternative model for dannelse av gneisdomer (MSc thesis). University of Bergen.
Larsen, O., Fossen, H., Langeland, K., Pedersen, R.B., 2003. Kinematics and timing of polyphase post-Caledonian deformation in the Bergen area, SW Norway. Norw. J. Geol. 83, 149–165.
Li, Z.X., Bogdanova, S.V., Collins, A.S., Davidson, A., De Waele, B., Ernst, R.E., Fitzsimons, I.C.W., Fuck, R.A., Gladkochub, D.P., Jacobs, J., Karlstrom, K.E., Lu, S., Natapov, L.M., Pease, V., Pisarevsky, S.A., Thrane, K., Vernikovsky, V., 2008. Assembly, configuration, and break-up history of Rodinia: a synthesis. Precambr. Res. 160, 179–210. http://dx.doi.org/10.1016/j.precamres.2007.04.021.
Ludwig, K.R., 1998. On the treatment of concordant uranium-lead ages. Geochim. Cosmochim. Acta 62, 665–676. http://dx.doi.org/10.1016/S0016-7037(98)00059-3.
Ludwig, K.R., 2003. User's Manual For Isoplot 3.00: A Geochronological Toolkit for Microsoft Excel. Kenneth R. Ludwig.
Mezger, K., Krogstad, E.J., 1997. Interpretation of discordant U-Pb zircon ages: an evaluation. J. Metamorph. Geol. 15, 127–140. http://dx.doi.org/10.1111/j.1525-1314.1997.00008.x.
Milnes, A., Wennberg, O., Skår, Ø., Koestler, A., 1997. Contraction, extension and timing in the South Norwegian Caledonides: the Sognefjord transect. Geol. Soc. London Spec. Publ. 121, 123–148.
Möller, C., Bingen, B., Andersson, J., Stephens, M.B., Viola, G., Schersten, A., 2013. A non-collisional, accretionary Sveconorwegian orogen – comment. Terra Nova 25, 165–168. http://dx.doi.org/10.1111/ter.12029.
Möller, C., Andersson, J., Dyck, B., Antal Lundin, I., 2015. Exhumation of an eclogite terrane as a hot migmatitic nappe, Sveconorwegian orogen. Lithos 226, 147–168. http://dx.doi.org/10.1016/j.lithos.2014.12.013.
Norton, M.G., 1987. The Nordfjord-Sogn Detachment, W Norway. Nor. Geol. Tidsskr. 67, 93–106.
Osmundsen, P.T., Andersen, T.B., 2001. The middle Devonian basins of western Norway: sedimentary response to large-scale transtensional tectonics? Tectonophysics 332, 51–68. http://dx.doi.org/10.1016/S0040-1951(00)00249-3.
Osmundsen, P.T., Braathen, A., Sommaruga, A., Skilbrei, J.R., Nordgulen, O., Roberts, D., Andersen, T.B., Olesen, O., Mosar, J., 2005. Metamorphic core complexes and gneiss-cored culminations along the Mid-Norwegian margin: an overview and some current

ideas. Norw. Petrol. Soc. Spec. Publ. 12, 29–41. http://dx.doi.org/10.1016/S0928-8937(05)80042-6.
Pascal, C., Rudlang, T., 2016. Discovery of highly radioactive granite in the Bergen Region. Norw. J. Geol. 96, 319–328. https://doi.org/10.17850/njg96-4-03.
Pease, V., Daly, J.S., Elming, S.Å., Kumpulainen, R., Moczydlowska, M., Puchkov, V., Roberts, D., Saintot, A., Stephenson, R., 2008. Baltica in the Cryogenian, 850–630Ma. Precambr. Res. 160, 46–65. http://dx.doi.org/10.1016/j.precamres.2007.04.015.
Pedersen, R.B., Dunning, G.R., 1997. Evolution of arc crust and relations between contrasting sources: U-PL (age), Nd and Sr isotope systematics of the ophiolitic terrain of SW Norway. Contrib. Miner. Petrol. 128, 1–15. http://dx.doi.org/10.1007/s004100050289.
Pedersen, R.B., Bruton, D.L., Furnes, H., 1992. Ordovician Faunas, Island Arcs and Ophiolites in the Scandinavian Caledonides. Terra Nova 4, 217–222. http://dx.doi.org/10.1111/j.1365-3121.1992.tb00475.x.
Ragnhildstveit, J., Helliksen, D., 1997. Geologisk Kart Over Norge, berggrunnskart Bergen – M 1:250.000. Norges Geologiske Undersøkelse.
Rino, S., Kon, Y., Sato, W., Maruyama, S., Santosh, M., Zhao, D., 2008. The Grenvillian and Pan-African orogens: world's largest orogenies through geologic time, and their implications on the origin of superplume. Gondwana Res. 14, 51–72. http://dx.doi.org/10.1016/j.gr.2008.01.001.
Roberts, D., 2003. The Scandinavian Caledonides: event chronology, palaeogeographic settings and likely, modern analogues. Tectonophysics 365, 283–299. http://dx.doi.org/10.1016/S0040-1951(03)00026-X.
Roberts, N.M.W., Slagstad, T., 2015. Continental growth and reworking on the edge of the Columbia and Rodinia supercontinents; 1.86-0.9 Ga accretionary orogeny in southwest Fennoscandia. Int. Geol. Rev. 57, 1582–1606. http://dx.doi.org/10.1080/00206814.2014.958579.
Roberts, N.M.W., Slagstad, T., Parrish, R.R., Norry, M.J., Marker, M., Horstwood, M.S.A., 2013. Sedimentary recycling in arc magmas: geochemical and U-Pb-Hf-O constraints on the Mesoproterozoic Suldal Arc, SW Norway. Contrib. Miner. Petrol. 165, 507–523. http://dx.doi.org/10.1007/s00410-012-0820-y.
Roberts, N.M.W., Slagstad, T., Viola, G., 2015. The structural, metamorphic and magmatic evolution of Mesoproterozoic orogens. Precambr. Res. 265, 1–9. http://dx.doi.org/10.1016/j.precamres.2015.05.031.
Roffeis, C., Corfu, F., 2014. Caledonian nappes of southern Norway and their correlation with Sveconorwegian basement domains. Geol. Soc. London Spec. Publ. 390, 193–221. http://dx.doi.org/10.1144/SP390.13.
Roffeis, C., Corfu, F., Gabrielsen, R.H., 2013. A Sveconorwegian terrane boundary in the Caledonian Hardanger-Ryfylke Nappe Complex: the lost link between Telemarkia and the Western Gneiss Region? Precambr. Res. 228, 20–35. http://dx.doi.org/10.1016/j.precamres.2013.01.008.
Rohr, T.S., Bingen, B., Robinson, P., Reddy, S.M., 2013. Geochronology of Paleoproterozoic Augen Gneisses in the Western Gneiss Region, Norway: evidence for Sveconorwegian Zircon Neocrystallization and Caledonian Zircon Deformation. J. Geol. 121, 105–128. http://dx.doi.org/10.1086/669229.
Root, D., Corfu, F., 2012. U-Pb geochronology of two discrete Ordovician high-pressure metamorphic events in the Seve Nappe Complex, Scandinavian Caledonides. Contrib. Miner. Petrol. 163, 769–788. http://dx.doi.org/10.1007/s00410-011-0698-0.
Root, D.B., Hacker, B.R., Mattinson, J.M., Wooden, J.L., 2004. Zircon geochronology and ca. 400 Ma exhumation of Norwegian ultrahigh-pressure rocks: an ion microprobe and chemical abrasion study. Earth Planet. Sci. Lett. 228, 325–341. http://dx.doi.org/10.1016/j.epsl.2004.10.019.
Rykkelid, E., Fossen, H., 1992. Composite fabrics in Midcrustal Gneisses – observations from the Oygarden complex, West Norway Caledonides. J. Struct. Geol. 14, 1–9. http://dx.doi.org/10.1016/0191-8141(92)90139-N.
Schulze, K., 2014. Radiogenic Heat Production in the Bed Rock of Bergen, Norway with Gamma-Spectrometry and its Relevance for Geothermal Energy (MSc thesis). Christian-Albrechts Universität Kiel, pp. 108.
Seranne, M., Seguret, M., 1987. The Devonian basins of western Norway: tectonics and kinematics of an extending crust. Geol. Soc. London Spec. Publ. 28, 537–548.
Skår, Ø., 2000. Field relations and geochemical evolution of the Gothian rocks in the Kvamsoy area, southern Western Gneiss Complex, Norway. Norges Geologiske Undersøkelse Bulletin 437, 5–24.
Skår, Ø., Pedersen, R.B., 2003. Relations between granitoid magmatism and migmatization: U-Pb geochronological evidence from the Western Gneiss Complex, Norway. J. Geol. Soc. 160, 935–946. http://dx.doi.org/10.1144/0016-764901-121.
Skår, Ø., Furnes, H., Claesson, S., 1994. Proterozoic orogenic magmatism within the Western Gneiss Region, Sunnfjord, Norway. Nor. Geol. Tidsskr. 74, 114–126.
Slagstad, T., Roberts, N.M.W., Marker, M., Rohr, T.S., Schiellerup, H., 2013a. A non-collisional, accretionary Sveconorwegian orogen. Terra Nova 25, 30–37. http://dx.doi.org/10.1111/ter.12001.
Slagstad, T., Roberts, N.M.W., Marker, M., Rohr, T.S., Schiellerup, H., 2013b. A non-collisional, accretionary Sveconorwegian orogen – reply. Terra Nova 25, 169–171. http://dx.doi.org/10.1111/ter.12028.
Slagstad, T., Pin, C., Roberts, D., Kirkland, C.L., Grenne, T., Dunning, G., Sauer, S., Andersen, T., 2014. Tectonomagmatic evolution of the Early Ordovician supra-subduction-zone ophiolites of the Trondheim Region, Mid-Norwegian Caledonides. Geol. Soc. London Spec. Publ. 390, 541–561. http://dx.doi.org/10.1144/SP390.11.
Slagstad, T., Roberts, N.M.W., Kulakov, E., 2017. Linking orogenesis across a supercontinent; the Grenvillian and Sveconorwegian margins on Rodinia. Gondwana Res. 44, 109–115. http://dx.doi.org/10.1016/j.gr.2016.12.007.
Slama, J., Pedersen, R.B., 2015. Zircon provenance of SW Caledonian phyllites reveals a distant Timanian sediment source. J. Geol. Soc. 172, 465–478. http://dx.doi.org/10.1144/jgs2014-143.
Spencer, C.J., Roberts, N.M.W., Cawood, P.A., Hawkesworth, C.J., Prave, A.R., Antonini, A.S.M., Horstwood, M.S.A., 2014. Intermontane basins and bimodal volcanism at the onset of the Sveconorwegian Orogeny, southern Norway. Precambr. Res. 252, 107–118. http://dx.doi.org/10.1016/j.precamres.2014.07.008.
Stacey, J.S., Kramers, J.D., 1975. Approximation of Terrestrial Lead Isotope Evolution by a 2-Stage Model. Earth Planet. Sci. Lett. 26, 207–221. http://dx.doi.org/10.1016/0012-821x(75)90088-6.
Steel, R., Siedlecka, A., Roberts, D., 1985. The Old Red Sandstone basins of Norway and their deformation: a review. In: Gee, D.G., Sturt, B.A. (Eds.), The Caledonide Orogen – Scandinavia and Related Areas. Wiley, Chichester, pp. 293–315.
Steiger, R.H., Jäger, E., 1977. Subcommission on geochronology – convention on use of decay constants in geochronology and cosmochronology. Earth Planet. Sci. Lett. 36, 359–362. http://dx.doi.org/10.1016/0012-821x(77)90060-7.
Steltenpohl, M., Hames, W., Andresen, A., Markl, G., 2003. New Caledonian eclogite province in Norway and potential Laurentian (Taconic) and Baltic links. Geology 31, 985–988. http://dx.doi.org/10.1130/g19744.1.
Sturt, B.A., Thon, A., 1978. Caledonides of southern Norway. Caledonian-Appalachian orogen of the North Atlantic region, IGCP project 27, pp. 39–47.
Sturt, B.A., Skarpenes, O., Ohanian, A.T., Pringle, I.R., 1975. Reconnaissance Rb-Sr Isochron Study in Bergen Arc System and Regional Implications. Nature 253, 595–599. http://dx.doi.org/10.1038/253595a0.
Sturt, B., Pringle, I., Ramsay, D., 1978. The Finnmarkian phase of the Caledonian orogeny. J. Geol. Soc. 135, 597–610.
Torsvik, T.H., Cocks, L.R.M., 2005. Norway in space and time: a centennial cavalcade. Norw. J. Geol. 85, 73–86.
Torsvik, T.H., Smethurst, M.A., Meert, J.G., VanderVoo, R., McKerrow, W.S., Brasier, M.D., Sturt, B.A., Walderhaug, H.J., 1996. Continental break-up and collision in the Neoproterozoic and Palaeozoic – a tale of Baltica and Laurentia. Earth Sci. Rev. 40, 229–258. http://dx.doi.org/10.1016/0012-8252(96)00008-6.
Tucker, R.D., Raheim, A., Krogh, T.E., Corfu, F., 1987. Uranium-lead zircon and titanite ages from the northern portion of the Western Gneiss Region, South-Central Norway. Earth Planet. Sci. Lett. 81, 203–211. http://dx.doi.org/10.1016/0012-821x(87)90156-7.
Tucker, R.D., Robinson, P., Solli, A., Gee, D.G., Thorsnes, T., Krogh, T.E., Nordgulen, O., Bickford, M.E., 2004. Thrusting and extension in the Scandian hinterland, Norway: new U-Pb ages and tectonostratigraphic evidence. Am. J. Sci. 304, 477–532. http://dx.doi.org/10.2475/ajs.304.6.477.
Vetti, V.V., Fossen, H., 2012. Origin of contrasting Devonian supradetachment basin types in the Scandinavian Caledonides. Geology 40, 571–574. http://dx.doi.org/10.1130/G32512.1.
Weiss, L.E., 1977. Structural features of the Laksevåg Gneiss, Bergen, Norway. Norges Geologiske Undersøkelse 334, 1–17.
Wennberg, O.P., 1996. Superimposed fabrics due to reversal of shear sense: an example from the Bergen Arc Shear Zone, western Norway. J. Struct. Geol. 18http://dx.doi.org/10.1016/0191-8141(96)00014-4. 871-&.
Wennberg, O.P., Milnes, A.G., 1994. Interpretation of kinematic indicators along the northeastern margin of the bergen arc system – a preliminary field-study. Nor. Geol. Tidsskr. 74, 166–173.
Wennberg, O.P., Milnes, A.G., Winsvold, I., 1998. The northern Bergen Arc Shear Zone – an oblique-lateral ramp in the Devonian extensional detachment system of western Norway. Nor. Geol. Tidsskr. 78, 169–184.
Whitehouse, M.J., Kamber, B.S., 2005. Assigning dates to thin gneissic veins in high-grade metamorphic terranes: a cautionary tale from Akilia, southwest Greenland. J. Petrol. 46, 291–318. http://dx.doi.org/10.1093/petrology/egh075.
Whitehouse, M.J., Claesson, S., Sunde, T., Vestin, J., 1997. Ion microprobe U–Pb zircon geochronology and correlation of Archaean gneisses from the Lewisian Complex of Gruinard Bay, northwestern Scotland. Geochim. Cosmochim. Acta 61, 4429–4438. http://dx.doi.org/10.1016/S0016-7037(97)00251-2.
Whitehouse, M.J., Kamber, B.S., Moorbath, S., 1999. Age significance of U-Th-Pb zircon data from early Archaean rocks of west Greenland – a reassessment based on combined ion-microprobe and imaging studies. Chem. Geol. 160, 201–224. http://dx.doi.org/10.1016/S0009-2541(99)00066-2.
Whitney, D.L., Teyssier, C., Vanderhaeghe, O., 2004. Gneiss domes and crustal flow. Geol. Soc. Am. Spec. Papers 380, 15–33. http://dx.doi.org/10.1130/0-8137-2380-9.15.
Whitney, D.L., Teyssier, C., Rey, P., Buck, W.R., 2013. Continental and oceanic core complexes. Geol. Soc. Am. Bull. 125, 273–298. http://dx.doi.org/10.1130/B30754.1.
Wiedenbeck, M., Alle, P., Corfu, F., Griffin, W., Meier, M., Oberli, F., Quadt, A.V., Roddick, J., Spiegel, W., 1995. Three natural zircon standards for U-Th-Pb, Lu-Hf, trace element and REE analyses. Geostand. Newslett. 19, 1–23. http://dx.doi.org/10.1111/j.1751-908X.1995.tb00147.x.
Wintsch, R.P., Christoffersen, R., Kronenberg, A.K., 1995. Fluid-rock reaction weakening of fault zones. J. Geophys. Res. Solid Earth 107http://dx.doi.org/10.1029/94jb02622. ECV 1-1-ECV 1-13.